CellPress

Matter

Review

Quasicrystalline materials from non-atom building blocks

Yasutaka Nagaoka,[1] Jeremy Schneider,[1] Hua Zhu,[1] and Ou Chen[1,*]

SUMMARY

The discovery of quasicrystals (awarded with the 2011 Nobel Prize in Chemistry) generated a revolutionary impact on crystallography, and hence a plethora of structural topics across a range of science, technology, engineering, art, and math (STEAM) disciplines. The unconventional feature of quasicrystalline structures, i.e., exhibiting rotational symmetry without continuous translational symmetry (lattice periodicity), completely redefined the existing framework of viewing and categorizing matter. While quasicrystal research began with the development of intermetallic alloys, quasicrystalline materials have since been created from building blocks across length scales. In this review, we focus on quasicrystalline materials produced from various non-atom building blocks. In the following, we showcase some unique properties and potential applications of such materials, ranging from photonic crystals metamaterials to architecture/art designs and time crystals.

INTRODUCTION

As the central heart of all structures, symmetry has been extensively studied throughout history leading to a number of important mathematical concepts.[1] One such important theory is group theory, notably developed by Abel and Galois,[1] which gave rise to some key crystallographic concepts such as space groups and the crystallographic restriction theorem (Scheme 1).[2] For a long time, it was believed that all crystallographic symmetries could be described by space group notation, and should follow the crystallographic restriction theorem.[2] For instance, the crystallographically allowed rotational symmetries in crystals were strictly limited to 2-, 3-, 4-, and 6-fold, while excluding all others.[2,3] However, this theory was challenged upon the first discovery of an icosahedral quasicrystal that can be described as a three-dimensional (3D) cut of a 6D hypercrystal structure.[4] In 1982, Dan Shechtman observed an astonishing electron diffraction (ED) pattern with a strictly forbidden 10-fold rotational symmetry from a rapidly solidified Al-Mn Intermetallic alloy sample,[4] which violated the crystallographic restriction theorem. After an almost 2-year scientific battle, the first quasicrystal publication written by Dan Shechtman appeared in *Physical Review Letters* in 1984.[4] The controversy surrounding the acceptance of quasicrystals among researchers finally led to categorizing of a new class of matter, i.e., quasicrystals, with neither crystalline lattices nor amorphous structures.[5–10] The distinctive structural characteristic of quasicrystalline (QC) order, also called quasiperiodicity, is the absence of continuous transitional periodicity; in other words, no unit cells, and the presence of crystallographically forbidden rotational symmetries. This counterintuitive structural definition caused quasicrystals to be considered a third category of crystallographic order in addition to the crystalline and non-crystalline categories.[2–11] Such a fundamentally new conception of matter drew a significant number of experimental efforts, which subsequently

PROGRESS AND POTENTIAL

Quasicrystals were thought to be impossible crystals before their discovery. Dan Shechtman first discovered a quasicrystal exhibiting an astonishing 10-fold symmetrical electron diffraction pattern, which was a forbidden symmetry according to crystallographic restriction theorem. Subsequent research delineated quasicrystalline order as an emerging third structural category besides crystalline order and randomness. To date, researchers have utilized various non-atom building blocks, such as molecules and nanoparticles, to create a spectrum of materials with different quasicrystalline lattices. Besides fascinating structural features, materials with quasicrystalline order show unique properties and hold promise for various applications. This review summarizes advances of quasicrystalline materials produced from non-atom building blocks.

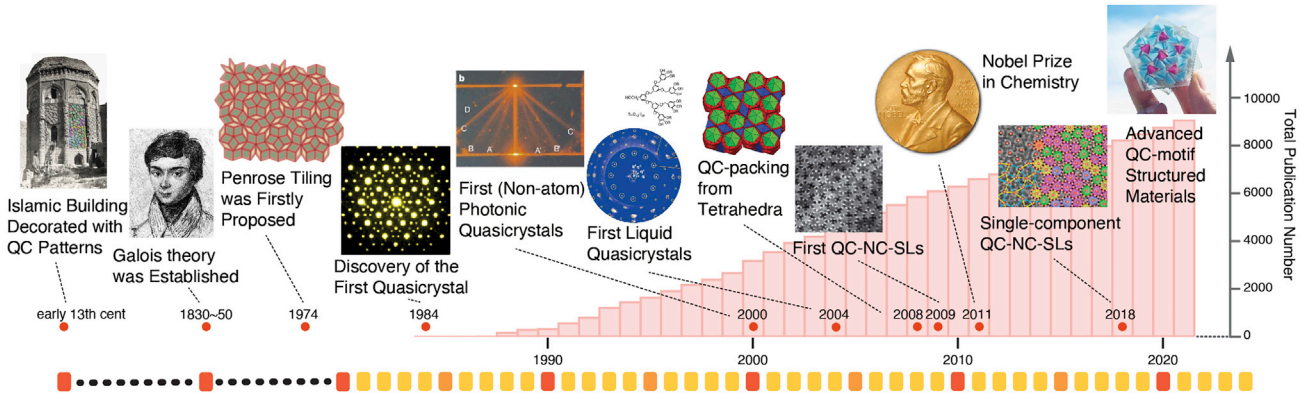

Scheme 1. Important events related to quasicrystals and quasicrystalline materials research

The important research related to quasicrystals and quasicrystalline materials is organized in a chronological order. The background plot describes the total number of publications citing "quasicrystal" since Dan Shechtman's Physical Review Letters in 1984, according to *Web of Science*. The panels used in this schematic (from left to right) were reproduced from Lu et al.,[140] Zoorob et al.,[114] Zeng et al.,[53] Haji-Akbari et al.,[77] Talapin et al.[41] ®© The Nobel Foundation, Nagaoka et al.,[22] Man et al.,[30] with permission. The Galois drawing is in the public domain.

resulted in discoveries of various intermetallic alloys exhibiting 8-, 10-, and 12-fold QC order.[12–15]

Although the QC phase was first discovered in an Al-Mn alloy and was later found in a variety of other intermetallic alloys, QC materials produced from non-atom building blocks (denoted as non-atom QC materials or NA-QC materials in this review, and defined as materials with a QC structure that are not constructed from atoms) have become an exciting research area in recent decades (Schematic 1). The long-range aperiodic order with forbidden rotational symmetries along with the unconventional properties induced by such unique structural features have opened burgeoning research avenues in chemistry, solid-state physics, materials science, and beyond. To date, NA-QC materials have been produced in a range of systems with wide length scales (from nanometer range to macroscopic objects), in various dimensions (e.g., Euclid space and timescale), using different fabrication methods (e.g., self-assembly, lithography), and exhibiting unconventional optical, magnetic, and other properties and functions.

Considering the number of excellent review articles and textbooks written about atomic quasicrystals (focusing on intermetallic alloy quasicrystals),[8,10,12–21] this review article focuses on state-of-the-art NA-QC materials and discusses the advantages of QC motifs for designing and engineering materials. We include brief explanations of QC order fundamentals; however, readers are encouraged to read other published review papers and textbooks for comprehensive understanding.[8–10,12–21] The outline of this review is as follows: in the first section, "QC structures and tessellations," we introduce important structures with QC order and the corresponding geometrical interpretations (tessellation and tiling rules); in the second section, "self-assembled QC materials from non-atom building blocks," we review materials with QC order self-assembled from non-atom building blocks, including nanocrystals (NCs), DNA, and organic or organometallic molecules. We also highlight some recent studies about the crystallization processes of NA-QC self-assemblies and discuss the insights acquired from these studies. In the third section, "novel properties from materials with QC order," we discuss a range of materials and objects integrated with QC architectures, such as photonic quasicrystals, metamaterials, frustrated magnets, art and architectural designs, and QC structures in

[1]Department of Chemistry, Brown University, Providence, RI, USA

*Correspondence: ouchen@brown.edu

https://doi.org/10.1016/j.matt.2022.09.027

unconventional dimensions, e.g., optical lattices and time crystals. Finally, we conclude by providing some of our prospects for this fascinating research topic.

QC STRUCTURES AND TESSELLATIONS

In this section, we will explain some of the major QC structures, including the 1D-QC order of the Fibonacci sequence, 2D 8-fold QC order with the Ammann-Beenker tiling, 10-fold QC order with the Penrose tiling, 12-fold QC order with square-triangle tiling, and the 3D icosahedral QC order with Ammann tiling. We also describe how to distinguish related structures that often assemble alongside QCs because of structural similarity to rigid QC structures, such as QC-approximant structures, random tiling motifs, and Frank-Kasper structures.

1D-QC order: The Fibonacci sequence

A 1D-QC order is an aperiodic sequence that can be defined by a recurrence equation. Among several 1D-QC motifs such as the Pell sequence (also known as Octonacci sequence), the squared Fibonacci sequence, and the Prouhet-Thue-Morse sequence (see Steurer and Deloudi[21] for more detailed information), the Fibonacci sequence is the most widely studied for QC materials. The Fibonacci sequence is formulated as $F_{n+2} = F_{n+1} + F_n$, and, when using binary digits as initial values F_0: L (black bars, Figure 1A) and F_1: S (red bars, Figure 1A), the sequence evolves as F_0: L, F_1: S, F_2: LS, F_3: LSL, F_4: LSLLS, F_5: LSLLSLSL,… The Fibonacci sequence exhibits several remarkable mathematical properties. For example, the "golden ratio" $\varphi = \frac{1+\sqrt{5}}{2} = 1.618034\ldots$, a ratio first studied by ancient Greek mathematicians and known as the most beautiful ratio,[21] can be obtained by convergence of F_{n+1}/F_n when *n* diverges to positive infinity irrespective of the initial given values of F_0 and F_1. There is also a fractal structure in the Fibonacci sequence (Figure 1B); i.e., structural recurrence at different magnification scales. Figure 1B shows the Fibonacci sequences from L and S with the length ratio of φ that is rescaled by 1/φ for each sequential step, keeping the same total length of the sequences (visually assisted with the vertical blue lines in Figure 1B), where a structural recurrence can be observed at various scales. It is also noteworthy that there is a set of discrete Fourier components despite the absence of periodicity in the Fibonacci sequence.[5] The existence of the discrete Fourier components is also supported by experimentally observed diffraction peaks of either 2D or 3D quasicrystals, which we will discuss in the sections "2D-QC structures" and "3D-QC order: Icosahedral quasicrystals with the Ammann tiling."

2D-QC structures

A 2D-QC order is a pattern where QC order exists only within a particular plane. Examples of 2D-QC structures include the 8-fold Ammann-Beenker tiling, the 10-fold Penrose tiling, and the 12-fold square-triangle tiling. These QC structures are summarized in this section using both experimental results and schematic tessellations.[23,24] In particular, the newly discovered flexible polygon tiling rule that can produce any arbitrary QC order with even-fold rotational symmetry will be discussed. Additionally, we also present some quasicrystal-related structures and clarify the differences from mathematically defined rigid QC structures.

Eight-fold QC order: Ammann-Beenker tiling

There have been numerous studies related to the geometry of the 8-fold QC order, including notable research by Robert Ammann, Frans Beenker, and Nicolaas Govert de Bruijn,[21] who successfully developed a substitution rule for obtaining octagonal tilings known as Ammann-Beenker tiling.[21] As illustrated in Figure 1C, two types of tiles (square and rhombus tiles with a sharper internal angle of 45°) are placed such that all the internal curves are connected through adjacent tiles (Figure 1C, top). The

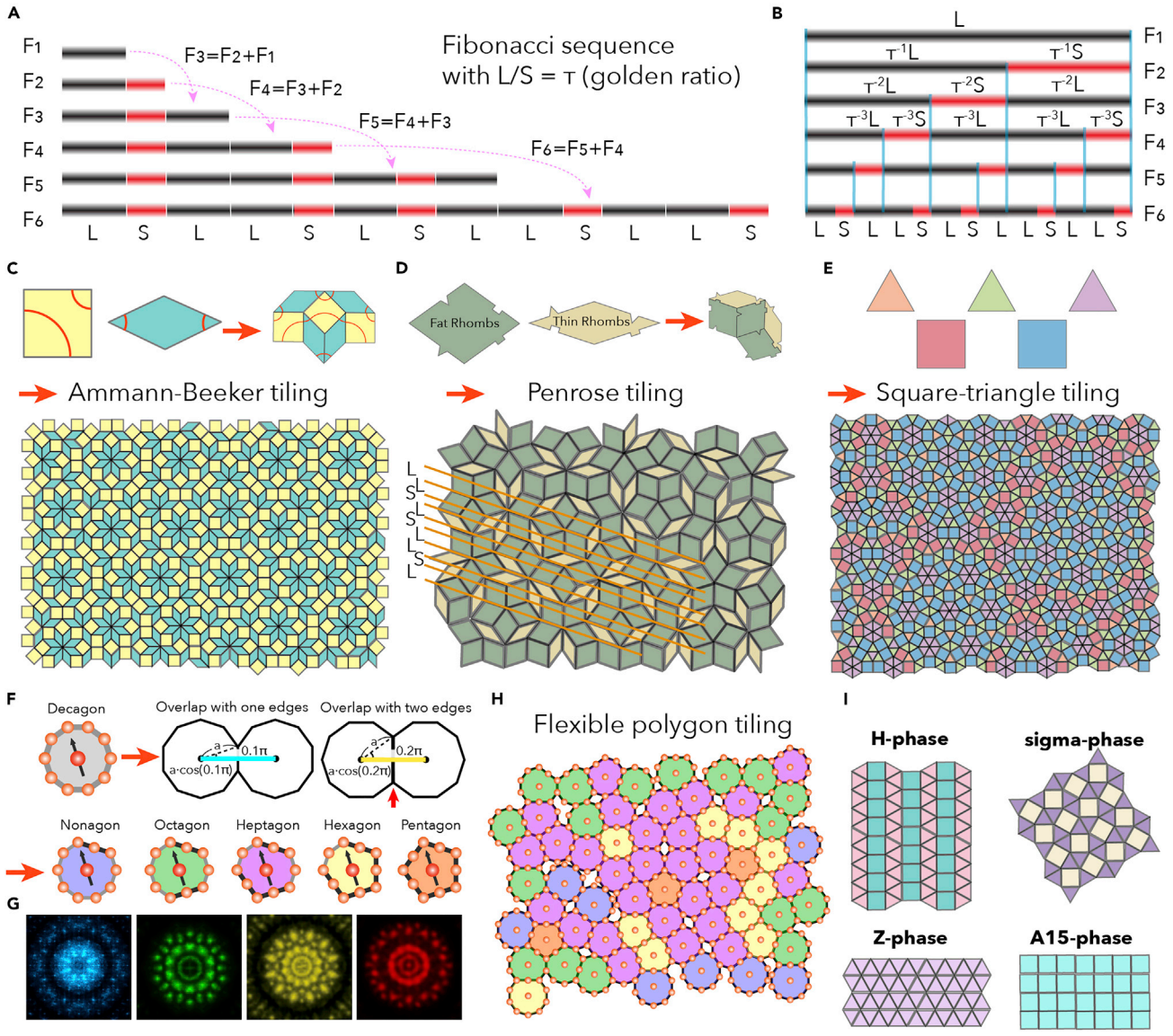

Figure 1. 1D- and 2D-QC order and tessellation

(A) Fibonacci sequence illustrated with long (black) and short (red) bars. The ratio of length (long/short) is adjusted to the golden ratio, τ.

(B) Fractal in the Fibonacci sequence. The total length of the Fibonacci sequences shown in (A) was normalized. The pale blue lines mark intervals in which recurrence of patterns (fractals) is observable.

(C) Ammann-Beeker tiling: (top left) square and rhombic tiles with red curves imposing the tiling rule, (top right) a fraction of Ammann-Beeker tiling, (bottom) a successful large Ammann-Beeker tiling.

(D) Penrose tiling: (top left) fat and thin rhombohedral tiles with notches and dents imposing the tiling rule, (top right) a fraction of Penrose tiling, (bottom) a large Penrose tiling.

(E) The square-triangle tiling: (top) five tiles used for the square-triangle tiling. The tiles were color coordinated by the substitution rule. (Bottom) A large square-triangle tiling.

(F) The flexible decagon transformation. The flexible polygon tiling rules allow polygons (decagons) to overlap with one (left) or two (right) edges. Regular decagon tiles are transformed into nonagons (nine edges), octagons (eight edges), heptagons (seven edges), hexagons (six edges), or pentagons (five edges) after the transformation process.

(G) FFT patterns of QCs made through the flexible polygon tiling operations from octagons, decagons, dodecagons, and tetradecagons (from left to right).

(H) A successful large flexible polygon tiling.

(I) Frank-Kasper structures constructed from square and/or triangle tiles; (top left) the elongated triangular tiling corresponding to H phase, (top right) the snub square tiling corresponding to Frank-Kasper sigma phase, (bottom left) the triangle tiling corresponding to Z (Zr_4Al_3) phase, and (bottom right) the square tiling corresponding to Frank-Kasper A15 phase.

Parts (F–H) were reproduced from Nagaoka et al.,[22] with permission.

resulting QC structure (Figure 1C, bottom) shows an 8-fold rotational symmetry without any transitional periodicity. A fractal pattern can be observed in the resulting QC structure, with an expansion rate of $1+\sqrt{2} = 2.41421\ldots$, which is the "silver ratio."[21] In the laboratory, 8-fold quasicrystals (also known as octagonal quasicrystals) have been created primarily by rapid quenching of intermetallic alloy systems such as V-Ni-Si or Cr-Ni-Si, which are all thermodynamically metastable.[8,25,26]

Ten-fold QC order: Penrose tiling

Kepler proposed one of the most prominent tilings with a 10-fold symmetry from regular pentagons, pentacles (star shape), and regular decagon and fused decagon, which Kepler referred to as "Monster" tiles.[27] This tiling method inspired one of the most important tilings for quasicrystalline order, the Penrose tiling, named after Sir Roger Penrose (Figures 1D and 1E). There are three versions of Penrose tiling, i.e., a pentagon-based tiling (P1), a kite and dart version of it (P2), and a rhomb tiling (P3). We used the Penrose rhomb tiling (P3) as an example, with a graphical presentation shown in Figures 1D and 1E. Two kinds of rhomb tile with sharp internal angles of 36° (slim) and 72° (fat) are arranged like a jigsaw puzzle as shown in Figure 1D.[21] In real samples, crystals with 2D 10-fold QC symmetry are called decagonal quasicrystals. Some experimentally synthesized decagonal quasicrystals such as Al-based quasicrystals and MgZn-based quasicrystals are known to be thermodynamically stable,[26] while metastable forms are also possible.[21,28] These 10-fold QC structures show some interesting mathematical features, including the golden ratio between the two "lattice" spacings (L and S) (yellow lines in Figure 1D) and the Fibonacci sequence found along the 10-fold axis (Figure 1D). This is reflected in their diffraction patterns in reciprocal space and in their material properties that will be further explored in section "3D-QC order: Icosahedral quasicrystals with the Ammann tiling."

Twelve-fold QC order: Square-triangle tiling

There are several 12-fold QC tiling methods, including dodecagonal Socolar tiling and dodecagonal rhomb tiling.[21] Among them, the square-triangle tiling is most important, which uses regular triangle and square tiles to form 12-fold QC patterns (Figure 1F). In terms of their local tiling neighbors, the tiles can be further classified into three types of triangles and two types of squares (Figure 1F).[21] In the square-triangle tessellation, a fractal can be observed, which is especially important for differentiating a QC order from related QC approximants, random tiling structures, and Frank-Kasper phases that are created by the same tiles (see section "QC approximants and Frank-Kasper phases"). Most reported 12-fold quasicrystals (i.e., dodecagonal quasicrystals) are thermodynamically metastable,[26] with rare exceptions.[29] The 12-fold quasicrystals are structurally similar to some Frank-Kasper phases (see section "QC approximants and Frank-Kasper phases"), so they often coexist in real materials.[20]

Flexible polygon tiling rule

A new member of the QC tessellation methods called the flexible polygon tiling rule, has been recently proposed by the Chen group (Figures 1F–1H).[22] In contrast to all other QC tessellations that were mathematically developed prior to experimental observations, the flexible polygon tiling rule was derived from real-sample observation of NC superlattices (SLs) assembled from truncated tetrahedral quantum dots (TTQDs, also see section "QC SLs self-assembled from colloidal NCs").[22] Interestingly, this flexible polygon tiling rule shared some similarity with Kepler's Monster tilings[27] because two decagonal tiles can be transformed into a monster by making the overlapped area flat. The flexible polygon tiling rule generates unique QC structures as described by the following. The tiles for the flexible polygon tiling rule are

orientationally regulated regular polygons. These regular polygon tiles are placed randomly and densely with the condition that two neighboring polygons may overlap with one or two edges (Figure 1F, top), but no more than two edges. When overlapping with two edges between adjacent tiles, the outlines become flexible and are transformed into one straight line (denoted as a "flexible edge") (Figure 1F, top). As a result of this transformation, the allowed polygon tiles can only have a defined number of shape configurations. For example, starting with a decagon, five different polygons as shown in Figure 1F bottom with edge numbers of 5–9 can be obtained after transformation.[30] As a result, the flexible polygon tiling method creates uniquely ordered structures without continuous transitional symmetry (lattice periodicity) but with rotational symmetry as manifested in the fast Fourier transform (FFT) converted image (Figures 1G and 1H). This tiling method is robust enough to generate any arbitrary even-number-fold QC symmetries; e.g., the QC patterns with 8-, 10-, 12-, and 14-fold symmetries as shown in Figure 1G.[22]

QC approximants and Frank-Kasper phases

According to the rigorous definition, QC structures must possess a fractal order with rotational symmetry and no continuous translational symmetry (lattice periodicity). However, it is important to note that the term quasicrystals is often used loosely in experimental research, and it may refer to quasicrystal-related structures that do not strictly but largely follow certain QC tiling procedures, such as random quasicrystals, quasicrystals from random tiling, and quasicrystal approximants.[31,32] Due to high similarities of their local structures, quasicrystals and these related structures often result in similar reciprocal-space patterns such as ED patterns or FFT images, which makes it difficult to distinguish these structures. In addition, some Frank-Kasper phases are often compared with dodecagonal QC materials.[33] The Frank-Kasper phases of H, sigma, A15, and Z can also be expressed as tiling of squares and triangles, namely the elongated triangular tiling (Figure 1I, top left), the snub square tiling (Figure 1I, top right), the triangle tiling (Figure 1I, bottom left), and the square tiling (Figure 1I, bottom right), respectively.[34] As a consequence of their structural similarity, these Frank-Kasper phases commonly coexist with dodecagonal quasicrystals seen in experiments due to their comparable entropic-energy states.[33]

3D-QC order: Icosahedral quasicrystals with the Ammann tiling

3D-QC-ordered structures possess 2D-QC order in multiple crystal planes (Figures 2A and 2B), and the only known 3D-QC structure is the icosahedral quasicrystal.[15,21] The icosahedral quasicrystal structure contains six 5-fold axes, 10 3-fold axes, and 15 2-fold axes (Figure 2A).[4,15,21] These crystallographic features have been manifested by a series of rotational transmission electron microscopy (TEM) ED images showing 10-fold QC patterns from the six 5-fold axial projections and 3-fold and 2-fold patterns when orientating the sample along its 3- and 2-fold axes through proper rotations (Figure 2A).[4,35–37] The 10-fold symmetry ED patterns are the same as the one observed in decagonal quasicrystals and exhibit characteristic mathematical features such as pentagon expansion, a series of pentagons with the expansion ratio of the golden ratio φ, which can be drawn by constellating the dotted ED signals (green, blue, pink, and orange lines in Figure 2A). An icosahedron (Figure 2C, left) and its dual form, a dodecahedron (Figure 2C, right), are both geometrically appropriate shapes for representing these axes. Many icosahedral quasicrystals are stable enough to form single crystals in a decagonal shape, and Figure 2D shows a decagonal-shaped single crystal of a Ho-Mg-Zn icosahedral quasicrystal.[4,35–37] The icosahedral quasicrystal structures can be replicated through a block-stacking method called Ammann tiling (also known as 3D Penrose tiling)

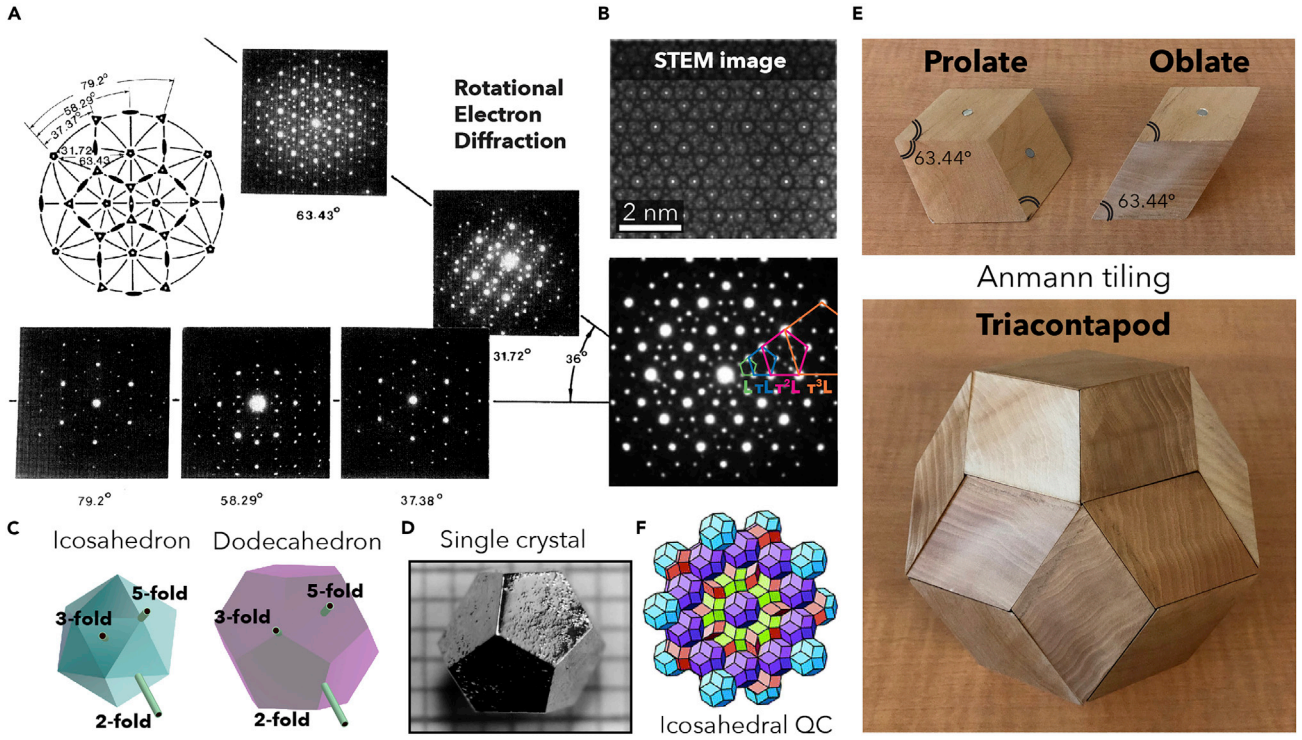

Figure 2. Icosahedral QC order and the Ammann tiling

(A) Selected-area electron diffraction patterns of an icosahedral quasicrystal from multiple projections: (top left) the stereographic projection, and (right bottom) an electron diffraction pattern with a 10-fold symmetry. A pentagon expansion was observed in the diffraction pattern as illustrated on the right.

(B) High-resolution TEM image of an Al-Pd-Mn icosahedral quasicrystal from the 10-fold axis.

(C) Icosahedron (left) and dodecahedron (right). The pale green poles are the rotational axes.

(D) Photograph of a single crystal of Ho-Mg-Zn icosahedral quasicrystals with a dodecahedron shape.

(E) The Ammann tiling: (top) prolate and oblate tiles, and (bottom) a constructed triacontahedron unit.

(F) An icosahedral structure reconstructed from larger Ammann tiling using computer models.

(A) Reproduced from Shechtman et al.[4] with permission.

(B) Reproduced from Yang et al.[35] with permission.

(D) Reproduced from Abe et al.[37] with permission. The wooden models shown in (E) were provided through the courtesy of Debora Coombs.

(F) Reproduced from Madison[40] with permission.

using two types of building blocks, prolate and oblate with golden rhombus faces (i.e., a rhombus with an acute sharper angle of 63.44°; Figure 2E top).[21,38,39] As a result of using 10 pieces each of prolate and oblate blocks, a rhombic triacontahedron can be constructed (Figure 2E), which can be further expanded into large 3D icosahedral QC structure by following the Ammann tiling method (Figure 2F).[40]

SELF-ASSEMBLED QC MATERIALS FROM NON-ATOM BUILDING BLOCKS

Self-assembly processes have been used to produce QC materials from a variety of non-atom building blocks, such as NCs,[22,41–46] organometallic molecules,[47–52] liquid-crystal molecules,[53–57] block-copolymers,[58–60] and biomolecules (e.g., DNA).[61] As these QC materials can incorporate microscopic functionalities from building blocks together with unique aperiodic macroscopic structures, they hold great promise for various potential applications. In this section, we discuss some important design principles that can lead to spontaneous QC order formation through self-assembly of non-atom building objects.

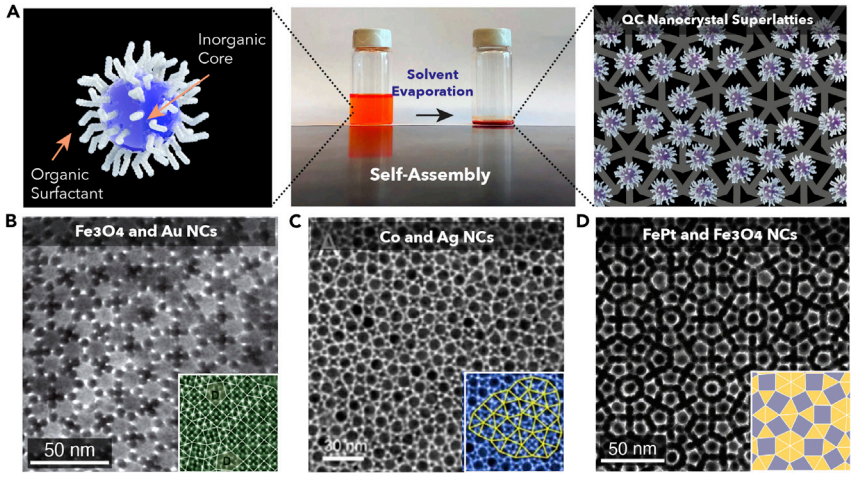

Figure 3. QC SLs from multiple kinds of NCs

(A) Schematic illustration of a NC and a QC NC SL: (left) NCs composed of inorganic cores and surfactant molecules. (Right) NCs are aligned in a QC order. (Middle) NCs are usually dispersed in a non-polar solvent, and SLs spontaneously form upon solvent evaporation.

(B–D) TEM images of QC binary NC SLs with 12-fold QC order and the corresponding tiling illustrations (inset). (B) QC NC SLs from Fe_3O_4/Au NCs and PbS/Pd NCs.[41,42] (C) QC NC SLs from magnetic Co/Ag NCs.[43] (D) QC NC SLs with 12-fold QC order from FePt/Fe_3O_4 NCs.[45]

(B) Reproduced from Talapin et al.[41] and Bodnarchuk et al.[42] with permission.

(C) Reproduced from Yang et al.,[43] with permission.

(D) Reproduced from Ye et al.[45] with permission.

QC SLs self-assembled from colloidal NCs

Colloidal NCs, nanosized inorganic crystals (~3–100 nm) passivated by surfactant molecules (Figure 3A left), often spontaneously arrange themselves into different types of arrays, i.e., NC SLs, upon solvent evaporation or controlled crystallization (Figure 3A).[62–66] The resulting structures often contain crystalline order comparable with atomic crystal structures[67–72]; however, NC SLs with unusual superstructures have been also reported,[73,74] including NC QC SLs (i.e., NC arrays with a QC order).[22,41–46]

QC binary-SLs from NCs

The first example of QC SLs was reported in 2009 by Talapin et al.[41] By using several combinations of two kinds of highly uniform NCs (i.e., Fe_3O_4 NCs and Au NCs; PbS NCs and Pd NCs), the authors achieved binary NC SLs with a 12-fold QC order (Figure 3B).[41] The entropic contribution is important in this formation mechanism because binary NC SLs tend to form superstructures with a high packing fraction.[65] In their study, the effective size ratio of ~0.43 between the two types of employed NCs was identified as the key requirement for forming QC SLs.[41] This size ratio led to the same packing fractions for AlB_2, CaB_6, and 12-fold QC structures. Thus, entropically, these structures were in similar energy states, resulting in appearance of AlB_2 and CaB_6 binary SL structures along with the 12-fold random QC SLs.[41] This strategy is robust enough to make more NC QC SLs, including those from different combinations of NCs,[42] and a combination of NCs with polyoxometalate.[44] In addition to entropy force, Yang et al. demonstrated that interparticle magnetic interactions can play an essential role in the random QC structure formation from Co and Ag NCs with an inorganic size ratio of ~0.49 (Figure 3C).[43] In their study, control experiments were conducted with ferromagnetic and paramagnetic Co NCs, demonstrating that the enthalpic term dictated by inter-Co-NC magnetic interactions may also play an essential role during QC formation.[43] Later in 2017, Ye et al.

produced QC NC SLs using two types of NCs with a size-ratio range of 0.60–0.66 (Figure 3D),[45] which were outliers compared with the previously reported examples.[41–44] The authors produced a set of 12-fold QC SLs from different NC combinations (e.g., Fe_3O_4 NCs, FePt NCs, $CoFe_2O_4$ NCs, and Au NCs) using a liquid-air interface method.[45] It should be noted that these NC QC SLs exhibited better quality in terms of crystal domain size and crystallinity compared with previous reports.[45] Using TEM and electron tomography, the obtained QC SLs were thoroughly characterized three dimensionally, which revealed QC SLs consisted of triangle and square subunits.[45] These subunits possessed structural bending in the z direction that affected local order surrounding each subunit, leading to the proposed partial matching rules for generating 12-fold NC QC SLs.[45] Furthermore, molecular dynamics computer simulations indicated the importance of interparticle interactions, particularly the attraction well width between neighboring NCs.[45] All of the reported QC structures found in binary NC SLs are categorized as random QC structures or quasicrystal approximants rather than perfect QC structures, mainly because the formation mechanism largely relies on entropic contribution (i.e., packing density).[41–45] Thus, recent studies focusing on the enthalpic mechanism (such as directional interaction and local matching rules) are especially important for producing perfect QCs comparable with atomic quasicrystal alloys with sufficient thermodynamic stability.[45,46,75]

Single-component QC SLs from TTQD NCs

In both theoretical and experimental studies, spontaneous formation of single-component quasicrystals was believed to be a challenge since normal objects are packed into periodic structures, such as cubic objects in simple cubic superstructures and spherical objects in *hcp* or *fcc*. In order to create unusual packing structures, one approach is to use non-spherical building blocks.[76] Glotzer's group investigated the packing order of many polygonal shapes and demonstrated that certain objects, such as square orthobicupola, square gyrobicupola, and augmented triangular prisms, cannot form ordered structures.[76] Tetrahedra are one of the simplest Platonic shapes, and yet can exhibit extremely unusual assembly behavior.[77–79] Aristotle's conjecture asserting that tetrahedra could completely fill space is one of the most important statements in the history of this field. This statement was later proved to be incorrect, and, conversely, tetrahedra have now been considered the convex shape possessing the lowest packing density when tiled in the 3D space of Euclidean geometry.[79] This claim was not disputed until 2008 when Haji-Akbari et al. found that regular tetrahedra could be packed with packing density reaching as high as 85.03% (more than 10% denser than close-packed spheres) with a QC-approximant structure.[77,78] In parallel, experimental efforts have also been made with tetrahedral and near-tetrahedral-shaped NCs showing peculiar self-assembly properties[80–82]; however, QC or QC-approximant structures were not reported until 2018.

In light of the previous research, in 2018, we reported that TTQD NCs could be packed into unconventional QC-related structures (Figure 4).[22,46] A series of complex superstructures have been successfully fabricated spanning from 1D tetrahelical arrays, 2D SL thin-film membranes, to 3D cluster-based single-supercrystals, and we resolved these unconventional structures with a high level of accuracy.[46] Our TTQD NC building blocks possess moderate shape truncations and anisotropic surface patchiness (localized ligand coverage profiles on different exposed NC surface facets) (Figure 4A),[46] which are imperative for induction of highly selective NC facet-to-facet connections and formation of unique assembled superstructures (Figures 4B–4F).[46] Notably, the obtained 2D SL thin-film possessed a

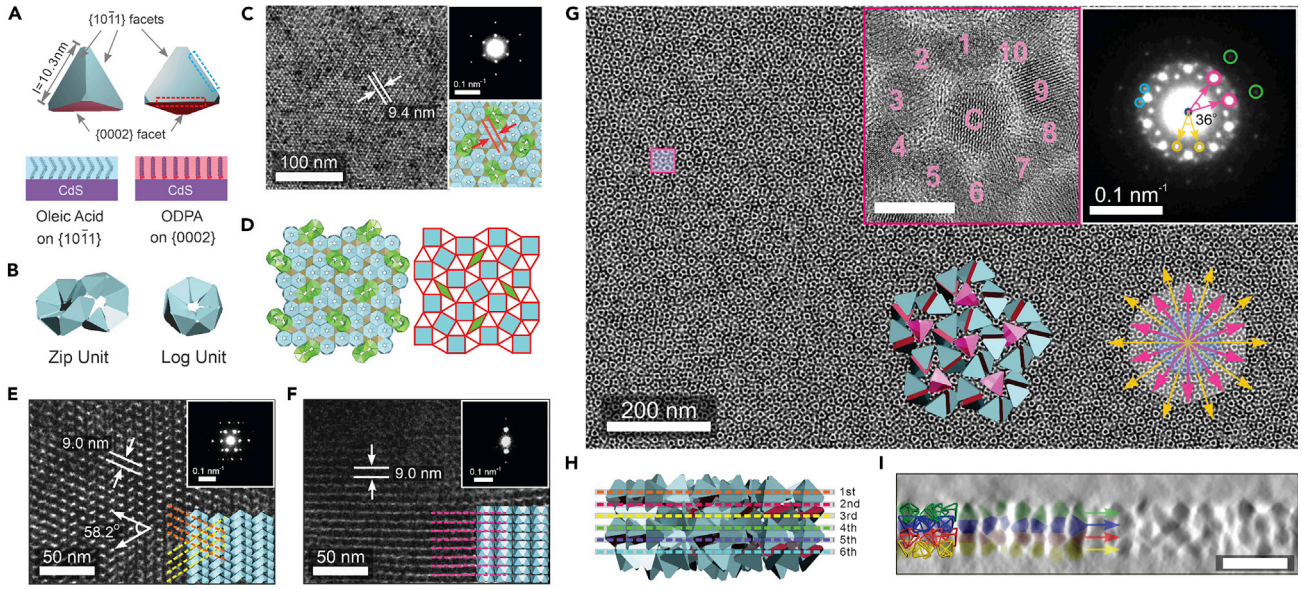

Figure 4. QC SLs from single-component truncated-tetrahedron-shaped NCs

(A) Schematic illustration of the effective tetrahedral shape of a TTQD. The TTQD exhibits three major [10 $\bar{1}$ 1] facets coated with oleic acid (blue) and one [0002] facet coated with octadecylphosphonic acid (ODPA, red).

(B) Subunits made from TTQDs. The zip units (left) and log units (right) are assembled into QC-approximant SLs.

(C) TEM image of QC-approximant SLs. The top-right inset is a small-angle electron diffraction (SAED) pattern. The bottom-right inset is a corresponding computer model.

(D) A corresponding computer model of QC-approximant SLs assembled from zip units and log units. For the sake of presentation, the zip units are colored in green.

(E) TEM image of the side view of the assembly formed from only zip units, and the corresponding SAED pattern (inset).

(F) TEM image of the side view of the assembly formed from only log units, and the corresponding SAED pattern (inset).

(G and H) (G) Representative TEM image of 10-fold QC SLs and (inset top right) the corresponding SAED pattern (pink, orange, and green cycles indicate 10-basis vectors; blue cycles indicate 20-basis vectors). The inset top left shows an HRTEM image of a decagon-derivative unit (square highlighted in the TEM image with 10 atomic domains on the framework and two in the center). Scale bar, 10 nm. The inset bottom left shows a computer-generated model of a double-decker QC-SL with six interconnected decagon-derivative units shown from a top view, and (H) from a side view.

(I) A vertical reconstruction slice of a double-decker QC-SL showing a four-layer TTQD stacking in the vertical direction (from top to bottom: green, blue, red, and yellow). Scale bar, 30 nm.

(A–F) Reproduced from Nagaoka et al.[22] with permission.

(G–I) Reproduced from Nagaoka et al.[46] with permission.

QC-approximant structure that could be well described via square-triangle tiling (Figures 4B–4D), showing some degree of agreement with the simulation predictions.[46,77,78] Within the structure, two types of basic packing subunits were identified: a log unit containing 12 TTQDs and a zip unit containing 20 TTQDs (Figure 4B),[46] both of which were close to the model proposed in the simulation work.[77,78] Later in the same year, we further demonstrated that a large-area QC SL with a novel 10-fold rotational symmetry could be assembled using the same TTQD building blocks at a liquid-air interface, a condition in which an enthalpic-force was in play during the assembly process rather than the exclusive entropy maximization pathway (Figures 4G–4I).[22] Electron tomography measurements with 3D structural reconstructions revealed that the SL exhibited a QC order in 2D lateral directions with a lamellar periodicity along the vertical direction (perpendicular to the substrate; Figures 4H and 4I). It is worth mentioning that QC lattices with a 10-fold rotational symmetry have been rarely seen, especially the ones stacked from non-atom building materials.[22] In order to describe the obtained novel 10-fold QC pattern, we proposed a new tiling rule, i.e., flexible polygon tiling rule, as discussed in the section "flexible polygon tiling rule." Further, mechanistic studies showed that

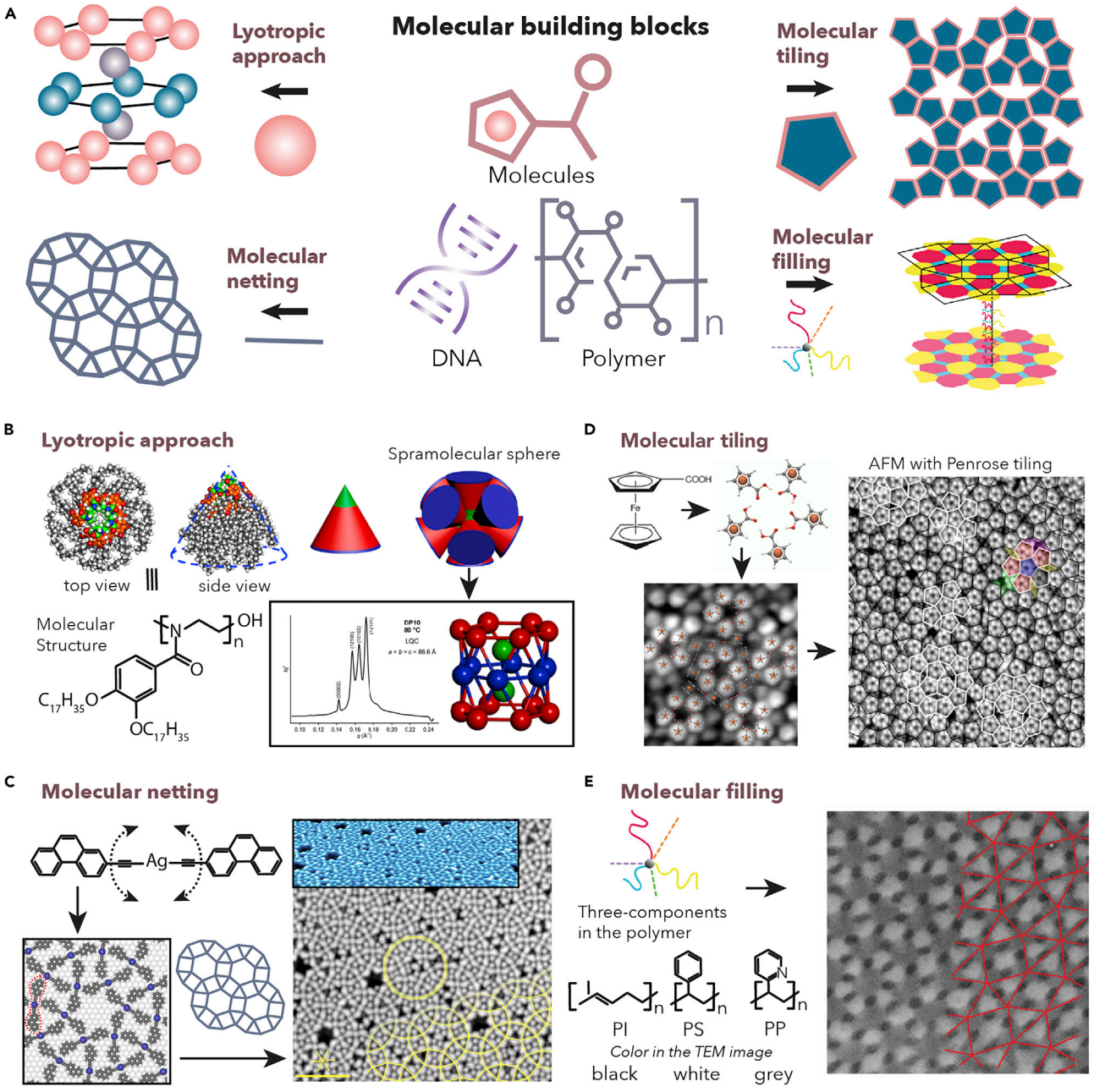

Figure 5. QC supramolecules

(A) Schematics of four QC supramolecule formation strategies: (top left) lyotropic approach, (bottom left) molecular netting approach, (top right) molecular tile approach, and (bottom right) molecular filling approach.

(B) Lyotropic approach: dendronized poly(2-oxazoline) molecules (bottom left) are in a cone shape as shown in the computer model (top left). Further mesostructures are formed from the cone-shaped molecules, e.g., supramolecular spheres (top right) and 12-fold liquid quasicrystals (bottom right). The QC structure was assessed by X-ray scattering as shown in the inset.

(C) Molecular netting approach: bis(phenanthren-2-yleythnyl)silver molecules (top left) were assembled in a QC order on a silver substrate (bottom left). The resulting 12-fold QC network was confirmed through STM measurements (right).

(D) Molecular tiling approach: pentagon subunits from five ferroceneacetic acid (left) are assembled on a gold substrate in a 10-fold QC (bottom left). The 10-fold QC order was observed in the STM images (right).

(E) Molecular filling approach: a three-component polymer composed of polyisoprene (PI), polystyrene (PS), and poly(2-vinylpyridine) (PP) segments (left) are self-assembled into a film with a 12-fold QC order as shown in the SEM (right).

The 12-fold QC pattern from (A) was reproduced from Zhang et al.[51] and Hayashida et al.[59] with permission.

Figure 5. *Continued*
(B) Reproduced from Holerca et al.[55] with permission.
(C) Reproduced from Zhang et al.[51] with permission.
(D) Reproduced from Wasio et al.[47] with permission.
(E) Reproduced from Hayashida et al.[59] with permission.

complex interplays among the applied liquid subphase, solvent molecules, and surface ligands of the TTQD NCs provided a deliberate environment to allow both entropic and enthalpic forces to act, which were additionally fueled by interparticle directional forces (induced by anisotropic patchiness) during the self-assembly process. This dynamic TTQD self-assembly system uniquely led to a series of unconventional stable/metastable superstructures including the unusual QC approximants and 10-fold QC SLs.[22]

QC supramolecules

With supramolecular chemistry, various nanoarchitectures can be created from organic and organometallic molecules, block-copolymers, and biomolecules such as DNA through delineated intermolecular interactions. Recently, researchers have proven that QC-ordered supramolecules are also feasible to obtain. In this section, we classified the QC self-assembly approaches for supramolecular species into four subsections as depicted in Figure 5A: (1) lyotropic approach, (2) molecular netting, (3) molecular tiling, and (4) molecular filling.

Lyotropic approach

It has been reported that several types of mesogen molecules can form lyotropic QC phases, also known as liquid quasicrystals.[53–57] In this approach, mesogens are designed to form a liquid-crystalline polymorph containing (12-fold) QC structures, which usually accompanies Pm $\bar{3}$ n, $P4_2/mnm$ and Im $\bar{3}$ m Frank-Kasper phases due to high structural similarity. The pioneering work conducted by Zeng et al., showed that a wedge-shaped dendric molecule (which they labeled as [3,4,5-$(3,5)^2$]12G_3CH_2OH) could form a 12-fold QC structure in addition to multiple lyotropic phases.[53] The liquid quasicrystal phase appeared as the ternary structure of mesogen molecules (a superstructure of supramolecular spheres from the mesogen illustrated in Figure 5B). Adequate interparticle interactions between supramolecular spheres was identified as key to the liquid quasicrystal formation, which was translated from the building block mesogen molecules. In addition to several noteworthy reports on liquid quasicrystals,[53,54,56] Holerca et al. recently presented an excellent mechanism regarding the formation of liquid quasicrystals from a series of dendronized poly(2-oxazoline) molecules (Figure 5B).[55] With different molecular chain lengths from 14 carbons to 17 carbons and polymerization degrees, n, from 5 to 100 (see left bottom of Figure 5B), various lyotropic phases formed, including a columnar structure, Frank-Kasper A15 and sigma phases, and a liquid QC structure.[55] Interestingly, lyotropic QC phases were only formed when dendronized poly(2-oxazoline) molecules with a chain length of 17 carbons and n of 5 were used, indicating quasicrystal liquid crystals can exist based on extremely delicate intermolecular interactions.[53,55] This lyotropic approach has been extended to create QC self-assemblies from cluster-based molecules. Yue et al. used silicon-oxide clusters coated with giant surfactants containing triazoles, esters, and styrenes, and studied their supramolecular structures.[54] A rich phase diagram depending on surfactant molecular identities was observed including lyotropic QC phases alongside lamellar, sigma-phase, double gyroids, bcc, and hexagonal phases.[54] The applications of liquid quasicrystals have been proposed widely in various applications such as sensors, photonics materials, and smart materials whose optical,

electrical, and mechanical properties can be controllably altered in response to external stimuli.[83]

Molecular netting

In the same way that 2D-QC patterns can be depicted by drawing lines on paper, some linear molecules can be deposited on substrates through self-assembly to form a QC order, which we call QC molecular nets here. Compared with typical 2D supramolecules assembled on substrates, QC molecular nets often possess much lower molecular density and structural rigidity, and thus the formation pathway is largely kinetically driven. Therefore, the building block molecules need to be designed to induce directional intermolecular interactions underpinned by molecular shape and configuration, as well as specific inter-molecule and molecule-substrate interactions. For instance, in 2016, Urgel et al. built a 12-fold QC molecular net by reticulating europium-(para-quaterphenyl-dicarbonitrile) molecules on a gold substrate.[49] Europium coordination chemistry enabled the co-existence of 4-, 5-, and 6-fold mononuclear coordination nodes, allowing some flexibility during the assembly process that led to the formation of 12-fold QC molecular nets.[49] Later in 2018, Zheng et al. reported another 12-fold QC molecular net assembled from bis(phenanthren-2-yleythnyl)silver organometallic molecules on a silver substrate (Figure 5C).[51] Several steps were required for the process from ethynyl-iodophenanthrene to the QC molecular net on silver substrate, including the predeposition of ethynyl-iodophenanthrene on the silver substrate, the reactions between ethynyl-iodophenanthrene and silver substrates to produce bis(phenanthren-2-yleythnyl)silver (see Figure 5C upper left), and annealing processes.[51] Moreover, silver ion inclusion and hydrogen transfer from the terminal alkyne to the dehalogenated site on the phenanthrene backbone contributed to QC net formation.[51] Aside from the organometallic chemistry, Mao et al. fabricated a 12-fold QC molecular net using biomolecules; i.e., programmed DNA.[61] The 12-fold QC molecular network formed from preassembled five-point star and six-point star nanomotifs made of DNA only when the nanomotifs were programmed to be structurally flexible.[61] Overall, the molecular net approach stresses the importance of controlled distortion due to designed steric hindrance and structural flexibility to avoid high-density packing structures.[84]

Molecular tiling

The molecular tiling approach uses planar molecules to create 2D-QC structures on substrates in a similar way to how tiles are arranged to create QC tessellations. Wasio et al. presented a beautiful example of molecular QC tiling from pentagon tiling units (i.e., five isomers of ferroceneacetic acids) deposited on a gold substrate (Figure 5D).[47] This is the only 10-fold QC supramolecule described to date, which is clearly visualized by scanning tunneling microscopy (STM) (Figure 5D right). To supplement experimental results, the authors also conducted theoretical density functional theory (DFT) calculations to further understand this abnormal QC formation process, finding that the pentagon tiling units were energetically metastable structures that need to be preserved for the QC supramolecular formation through delicate directional intermolecular interactions.[47,48] It should be noted that 10-fold 2D-QC structures can only be generated at a great cost of entropic-penalty due to their low tiling densities compared with possible competing crystalline structures or 12-fold QC structures; therefore, the kinetics of formation must be well incorporated.[47,48]

Molecular filling

Based on the controlled aggregation mechanism for block-copolymers and star polymers to form superstructures, the molecular filling approach uses polymers

that can form QC structures in their aggregates.[58–60,85] In 2008, a report by Zhang et al. showed the first example of a QC film produced from block-copolymers.[59] The tetrablock-polymers containing styrene, isoprene, styrene, and ethylene oxide were used for self-assembly into a 12-fold QC film, which was characterized by SAXS and TEM characterizations.[59] In 2012, Hayashida et al. reported another type of 12-fold QC pattern formed from an ABC star polymer containing polyisoprene, polystyrene, and poly(2-vinylpyridine) (see Figure 5E left). A QC film with a 12-fold symmetry was formed only when the ratio of these three components was adjusted to 1.0:2.7:2.5 (Figure 5E).[58] Following their own study, recently, the same group reported different QC structures from two kinds of block-copolymers with tetrablocks. By changing the mixing ratio of the two block-copolymers, the authors created 13 binary blend polymer films, and observed polymorphs including a double hexagonal pattern, a 3.3.4.3.4 Archimedean tiling pattern, and a 12-fold QC pattern.[60] In the molecular filling approach, the geometric and space-filling factors co-play a key role in favoring the formation of a QC order rather than any periodic ones.[58–60] These polymer films with nanoscale QC patterns are expected to exhibit unique mechanical properties owing to the lack of cleavable lattice planes.[20,86]

QC self-assembly formation mechanisms

One of the biggest challenges in quasicrystal research is to unveil formation mechanisms that cannot be explained by conventional crystallization theories such as QC nucleation, continuous growth without the guidance of a unit cell, and thermodynamic stability.[19,26] In parallel, a series of reports have suggested that NA-QC self-assemblies also go through complex steps like conventional periodic assemblies, although detailed mechanisms are far from clear yet. In this section, we try to summarize the current understanding of QC self-assembly mechanisms. On each topic, we will provide a systematic comparison of insights from atom QC self-assemblies, atomic quasicrystals, and theoretical studies to shed light on general requirements for QC formation.

Quasicrystallinity, growth front, and phason behavior

In this section, we discuss quasicrystal formation mechanisms in terms of the crystallinity of quasicrystals. A quasicrystal's crystallinity can be defined based on several aspects; for example, perfect quasicrystals versus random quasicrystals, crystal domains, and crystal defects. Instead of using a unit cell, a phason, a technical term for quasiparticle in quasicrystallinity, is commonly used to discuss crystallinity of quasicrystals. Phason behavior during quasicrystal formation was thought to be essentially important for quasicrystals' crystallization, yet the detailed mechanism is not fully understood.[87,88] Some theoretical studies have revealed the role of phason in determining the thermodynamic stability of quasicrystals. Engel et al. proposed the so-called phason flip model, which enables local fine structures in quasicrystals (i.e., local crystal configurations) to be flexibly changed, thereby providing additional entropic stability to ensure metastability of the entire system.[89] In this model, QC structures are expressed as tessellations from a set of polygon tiles as shown in Figure 6A, and some local configurations can be switched interchangeably as shown in Figure 6B.[89] In another theoretical study, by Achim et al., they described how to induce high quasicrystallinity by adjusting suitable thermodynamic conditions during the crystallization process.[90] This study indicated that conditions near the triple point (where three phases, i.e., gas, liquid, and solid, can coexist) are favorable for defect-free growth of quasicrystals, whereas random QC structures often form under conditions that are far from the triple point.[90] Experimentally, TEM *in situ* measurements of the growth of an Al-Ni-Co decagonal quasicrystal by Nagao et al. provided

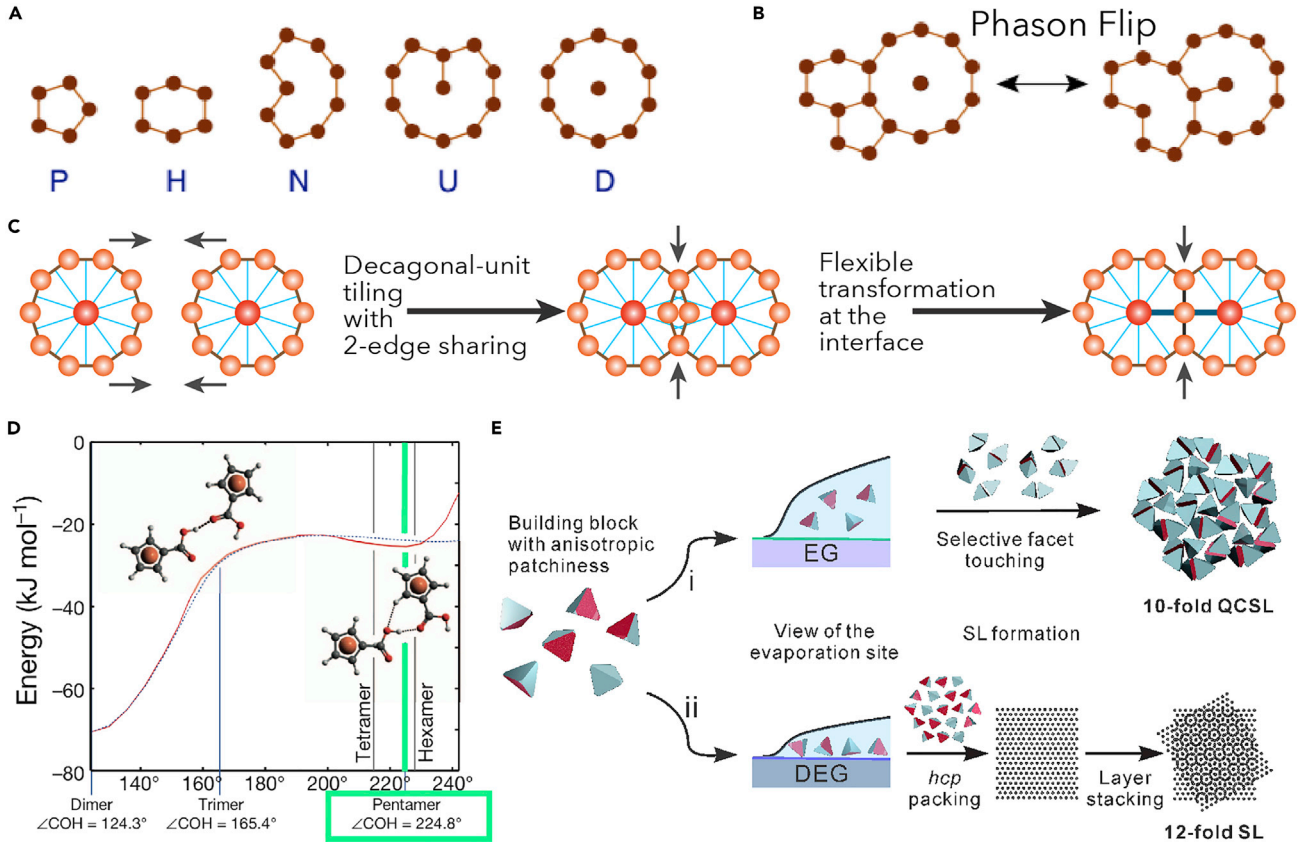

Figure 6. Mechanisms of NA-QC order formation

(A) Five phason-tiles in a simulated 10-fold QC order.

(B) Phason flip. QC structures could be created by tiling the phason-tiles shown in (A). Some local configurations can be interchangeably switched, which is called the phason flip.[89]

(C) The flexible polygon tiling rule. The interface between neighboring units is flattened.

(D) Metastability of QC supramolecules. A plot of calculated total cohesion energy between two ferroceneacetic acids as a function of the COH bond angle. The angle (224.8°) highlighted with green is consistent with the angle of the pentamer, validating the metastability of the pentamer and the QC supramolecules.[47]

(E) Schematic representation of the QC assembly pathways. (i) 10-fold QC SL formation on top of EG (ethylene glycol); (ii) hexagonal SL stacking formation on top of DEG.

(A and B) Reproduced from Engel et al.[89] with permission.

(C and E) Reproduced from Nagaoka et al.,[22] with permission.

(D) Reproduced from Wasio et al.[47] with permission.

direct observation of active phason behavior at the growth front, which caused frequent atomic rearrangements before complete incorporation (i.e., phason relaxation).[91] One of the most significant achievements is a recent finding by Shahani et al. that allowed crystal domain coalescence of quasicrystals, which could provide a general method to produce a giant single crystal.[92] Their study combined both theoretical and experimental results and revealed that phasons at the interface could facilitate crystal coalescence between adjacent crystal domains in a desired condition.[92]

In terms of non-atom building blocks, it has been suggested that phasons could also exist in NA-QC self-assemblies. We recently discovered a unique NC self-assembly behavior (i.e., flexible polygon tiling), which can be considered as an analogy to the concept of phason flip but at nanometer scale.[22] The interfacial flexibility in the flexible polygon tiling rule (i.e., sharing an edge between two

neighboring polygon units) is analogous to the phason flip configurational switches where tiles are flipped interchangeably at the interface (Figure 6C).[22] The origin of the flexible polygons assembled by TTQD NCs can be attributed to spatial margin in the decagonal units and the softness of organic surfactants on particle surfaces.[22] Evidently, we showed that when the surface surfactant molecules of the building blocks become stiffer in a more polar assembly environment, the NC QC SLs are longer be generated.[22] Although our study offered some mechanistic insights, more phason-type studies of such QC NC assemblies, taking advantage of the bigger size of the building blocks, are expected to provide more detailed QC nucleation and growth information. Besides, NA-QC self-assemblies with perfect QC order (rather than typically reported random QC order) may be required for more in-depth investigations of phason-type behaviors at the growth fronts of the materials.

Kinetics

It has been suggested that quasicrystallization involves multiple kinetic processes rather than a simple conversion from solute to crystals as classic crystallization theories depict.[93,94] Modern crystallization theory emphasizes the role of kinetics in crystallization and, in this context, researchers working with quasicrystals have also undertaken immense efforts to understand possible mechanisms.[95] Researchers have extensively studied several kinetic processes in QC crystallization, such as fine-tuning solute pair potentials, controlling interactions among solute, solvent and substrate, and refining crystallization conditions.[93,94] For example, a simulation study using the phase field crystal model with a two-length-scale potential performed by Jiang et al. discovered that nucleation and growth of dodecagonal quasicrystals could be driven by multiple kinetic processes.[94] The nuclei and an intermediate state, which can subsequently change into a QC order, are both transient and concurrent in their simulation. This transition process involving the intermediate state[94] is well in line with the modern crystallization theory,[95] which emphasizes the importance of a cloudy intermediate state before entering crystal nucleation stage.

In terms of QC materials from non-atom building blocks, previous reports have suggested that quasicrystallization involves kinetically driven steps under non-equilibrium conditions.[22,47–49,51,61] In the case of the ferrocene-based QC self-assemblies by Kandel's group (Figure 6D), thermodynamic stability dependence on the molecular angle between two ferroceneacetic acid molecules offered insight into the kinetic process (Figure 6D).[47,48] As shown in Figure 6D, ferroceneacetic acid molecules have a metastable state when adjacent molecules are placed at an orientational angle of 224.8°. Kinetically trapped pentamer units can only be formed when ferroceneacetic acid molecules were assembled with this condition, leading to a large 10-fold QC supramolecular network.[47,48] Otherwise, the final QC structure was replaced by a conventional thermodynamically stable dense structure.[48] In the case of 10-fold NC QC SLs, the anisotropic patchiness of the TTQDs induced by tetrahedron-like shape of the NCs and the directional patchiness (derived from the surfactant profile and intrinsic dipole moment of the Wurtzite crystal structure) guided the system to a kinetic assembly route instead of the common thermodynamic pathway.[48] Moreover, the system involved interactions that were found to be imperative during the formation process of the 10-fold QC SLs, where solvent and substrate combinations that minimally interrupted the inter-TTQD interactions were mandatory (Figure 6E).[22,96] Similarly, many of the stable atomic quasicrystals, i.e., stable icosahedral and dodecahedral quasicrystals, can only be formed with the assistance of directional atomic orbitals, analogous to the directional patchiness of the TTQD NCs.[8,22,75] By using other non-atom building blocks with designed

anisotropic and directional interactions, other QC structures formed through kinetic pathways can be anticipated.

NOVEL PROPERTIES FROM MATERIALS WITH QC ORDER

In addition to the fundamental studies discussed above, NA-QC motifs have also been integrated into state-of-the-art structured materials using methods such as lithography, 3D printing, and assembly at any scale. The QC-structured materials often exhibit unique properties, including optical,[97–104] lasing,[105–107] magnetic,[108–110] mechanical,[13,20,86] and electrical/thermal-conductivity properties.[111–113] This section features some fascinating examples such as photonic quasicrystals, QC metamaterials, and frustrated magnetic materials, which are followed by introducing some QC designs presented in artworks and architectures. We also discuss QC order in intangible dimensions such as optical QC lattices and time quasicrystals.

Photonic quasicrystals

Photonic crystals with a QC structure are called photonic quasicrystals, which can be distinguished from conventional photonic crystals by their distinctive structural colors and unique photonic band structures (Figure 7A).[97,98] In this section, a review of the fundamentals of 1D-, 2D-, and 3D-photonic quasicrystals is presented along with some promising application prospects.

1D-photonic quasicrystals

In contrast to conventional 1D-photonic crystals possessing periodic layers (Figure 7A left back), 1D-photonic quasicrystals consist of parallel alternating layers with a 1D-QC order (Figure 7A left front) and often exhibit more intricate photonic properties. While conventional photonic bandgaps of photonic crystals derive from the first Brillouin zone of the crystal structure, structural colors from 1D-photonic quasicrystals require different theoretical bases since QC structures do not have Brillouin zones in theory.[5] According to a theoretical study conducted by Kohmoto et al., the Bloch-like Fourier components of the Fibonacci sequences could lead to an unconventional "quasi-Brillouin zone" with the corresponding reciprocal vectors, thus photonic bandgaps.[116] Experimental confirmation of this theory was obtained as Gellermann et al. successfully fabricated 1D-photonic quasicrystals with alternating SiO_2 and TiO_2 layers following the Fibonacci sequence, which showed optical responses that were highly consistent with the theoretical prediction (Figure 7B).[115] Further 1D-photonic quasicrystals with distinct optical properties have been explored,[117] and expected application for 1D-photonic quasicrystals include optical filters[97] and sensing.[118]

2D-photonic quasicrystals

2D-photonic quasicrystals or QC photonic crystals are a class of 2D-photonic crystals possessing QC order (Figure 7A center front), in contrast to the conventional 2D-photonic crystals with periodic patterns (Figure 7A center back). Like other 2D-photonic crystals, 2D-photonic quasicrystals exhibit structural colors as a consequence of angle-dependent diffractions regulated by the Bragg-Snell law and oscillations of light both in the transverse-magnetic (TM) and electric (TE) mode.[97] Due to their QC structural features, 2D-photonic quasicrystals can exhibit unique photonic behaviors.[114,119–123] For example, Zoorob et al. fabricated air-hole patterns with a 12-fold QC order on a SiO_2/silicon nitrate substrate and observed interesting photonic properties (Figure 7C, left).[114] Upon passing the photonic quasicrystal film, incident light was complexly split into multiple beams in both TE and TM waves (Figure 7C, right), which were used to verify the existence of a photonic bandgap from QC periodicity with assistance from computer simulation.[114] Segev et al. conducted

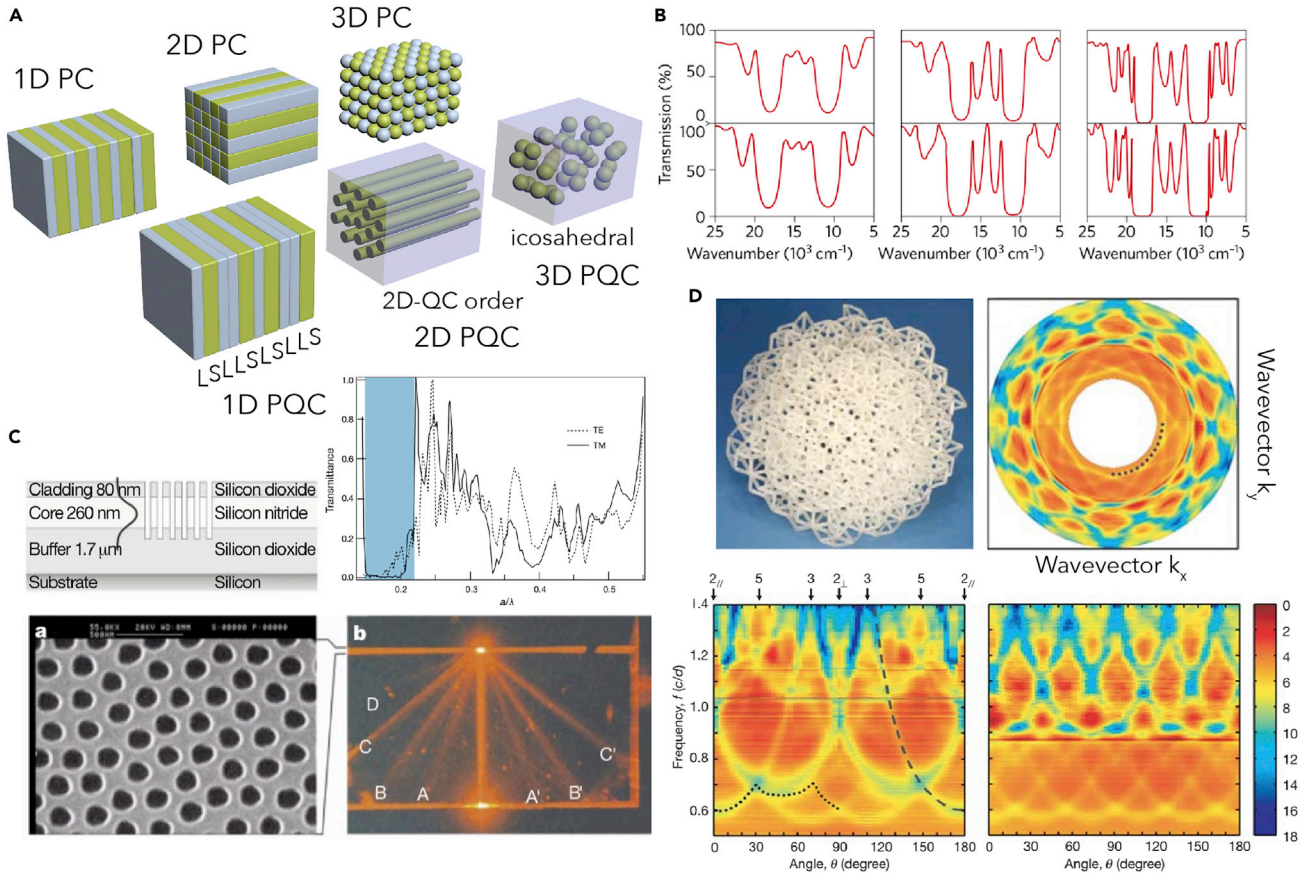

Figure 7. Photonic quasicrystals

(A) Schematics of 1D-, 2D-, and 3D-photonic crystals (PC) (back, from left to right) and photonic quasicrystals (PQC) (front, from left to right).

(B) Optical transmission spectra of 1D-PQCs: the experimental (top) and calculation results (bottom).[97] Evolution of the transmission spectra based on the number of the layer (F_6 to F_8 where F_n is the nth Fibonacci sequence.).

(C) 2D-PQC composed of silicon nitride and silicon dioxide.[114] (Top left) Schematic illustration of the 2D-PQC, (bottom left) SEM image of the 2D-PQC from the top-view, (bottom right) a photograph of split beams upon passing the 2D-PQC, and (top right) transmission spectra of TE and TM modes from the 2D-PQC.

(D) 3D-PQC made from plastic rods. (Top left) Photograph of the 3D-PQC. (Bottom) Transmission spectra as a function of frequency (y axis) and rotational angles along the 2-fold rotation axis (x axis) (left bottom) and along the 5-fold rotation axis (right bottom). (Top right) The calculated effective Brillouin zone of the 3D-PQC.

(B) Reproduced from Vardeny et al.[97] with permission. The original data are from Gellermann et al.[115]

(C) Reproduced from Zoorob et al.[114] with permission.

(D) Reproduced from Man et al.[30] with permission.

another notable study to emphasize the distinct difference between conventional and QC photonic crystals.[123] In general, the more structural disorder there is in photonic crystals, the more light is trapped (i.e., Anderson localization phenomenon).[97,98] However, in their report, the authors demonstrated that photonic quasicrystals could work oppositely.[123] Using a technique called optical induction, they created a series of 2D-photonic quasicrystals with controlled disorder levels, and demonstrated that the increased disorder level can influence the localized states near the pseudo-gap in these photonic quasicrystals, thus enabling finite-time, diffusive-like transport with enhanced wave transport property.[123]

3D-photonic quasicrystals

QC icosahedral structures can also be integrated into photonic crystals to produce 3D-photonic quasicrystals (Figure 7A, right). Interestingly, in spite of the absence

of Brillouin zones, 3D-photonic quasicrystals can display structural colors.[30,124,125] The first experimental demonstration was made by Man et al. in 2005 using a 3D model with an icosahedral QC structure crafted using plastic rods (length = 1 cm and diameter = 0.15 cm) (Figure 7D top left).[30] The photonic responses (transmission and reflection) in the microwave range were assessed from various projections (Figure 7D, bottom),[30] showing characteristic transmission spectra with a 5-fold (Figure 7D, bottom right) and 2-fold symmetry (Figure 7D, bottom left) along the 5-fold and 2-fold axes of the icosahedral structure, respectively.[30] Based on the observed spectra, the effective Brillouin zone for an icosahedral structure was backcalculated and depicted as a triacontahedral pattern, as shown in Figure 7D.[30]

Plasmonic quasicrystals and QC metamaterials

QC structures have been also incorporated into plasmonic material arrays (plasmonic quasicrystals), and researchers have found that such arrays exhibit unique plasmonic properties due to their plasmon coupling.[126–133] For example, Dal Negro's group fabricated aperiodic arrays of gold disks with a thickness of 30 nm and a diameter of 200 nm, and demonstrated that the arrays showed a broad scattering response covering the entire visible spectrum.[127,128] Lack of periodicity plays an important role for this unique photonic response as the plasmon coupling cannot be determined as it is in periodic systems, and thus scattering can be suppressed.[127] Such broadband plasmon resonances of plasmonic quasicrystals are expected to show advantages when applied for broadband sensors, light absorbers, and so forth.[127–130]

Metamaterials are materials with finer design structures than the wavelength of interest, which can guide light in unconventional ways. Left-handed materials and negative refractive index are representative of the physical properties of metamaterials, which have been studied in the fields of material science, physics, engineering, photonics, and nanoscience.[131–135] This field attracted immense attention because of the promising potential of these materials for important applications including far-infrared sensing, optical holography, cloaking, and planar metalenses.[131–135] Especially, plasmonic materials are often used in metaatoms as they can exhibit negative dielectric constants via surface plasmon phenomena.[131–133] As well as the internal designs of metaatoms (e.g., metal-dielectric-metal [MDM] and split ring resonator [SRR]), the arrangement of metaatoms is often extensively investigated in order to induce effective symmetry breaking optical behaviors.[99–102,130] For this reason, QCs are often incorporated in metamaterials' arrangement. Within this context, metasurfaces are metamaterials with 2D-arrangement, and QC metasurfaces (i.e., 2D QC arrangements of metaatoms) exhibit distinct photonic responses as the aperiodic QC arrangements of metaatoms can impart unique light diffraction and scattering properties.[99–102] Kruk et al. studied the transmission and circular dichroism (CD) spectra of Penrose-patterned QC metasurfaces made from MDM metaatoms of gold disk with a thickness of 25 nm and a diameter of 180 nm, and MgF_2 with a thickness of 30 nm.[99] Compared with periodic and amorphous metasurfaces, QC metasurfaces exhibited strong magnetic and electric field resonance in the transmission spectrum and suppressed sporadic scattering and weak CD responses, indicating that QC metasurfaces can simultaneously achieve isotropic optical response due to the weak diffraction signals as well as excellent metamaterial optical responses owing to the existent local order (e.g., magnetic and electric field resonance).[99] The principle is adapted to other QC metasurfaces that exhibit unique metamaterial

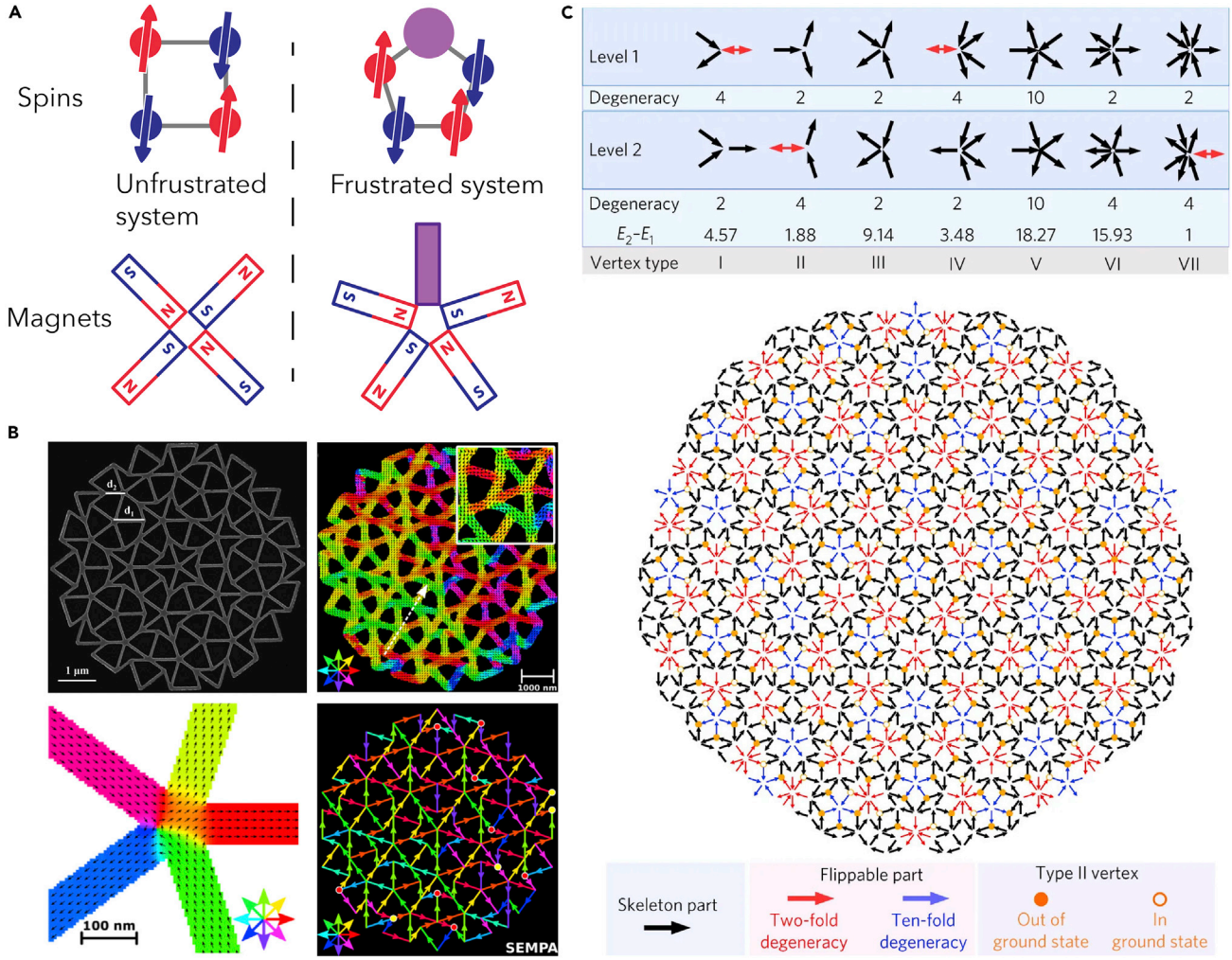

Figure 8. Frustrated magnetic materials with QC architectures

(A) Schematics of unfrustrated (left)/frustrated (right) systems of magnetic spin (top)/magnet (bottom). In frustrated systems, the location colored with purple could not determine the spin direction (or magnet polarization).

(B) QC-ordered magnetic lattice from permalloy: (top left) SEM image, (top right) SEMPA image, (bottom left) coarse-grained dipole map showing Ising polarizations defined by colored arrows, and (bottom right) magnetic texture at a pentagonal cross simulated by Object Oriented Micro Magnetic Framework.[108]

(C) A Penrose tiling pattern made from permalloy showing magnetic frustration:[110] (top) magnetic dipole configurations at vertices with the lowest (level 1) and second lowest (level 2) energy states with degeneracy; (bottom) the lowest energy configuration map of a magnetic QC network. The black arrows represent the skeleton parts that possess defined magnetic dipole directions, while the red and blue arrows represent flippable parts that degenerate the energetic state.

(B) Reproduced from Farmer et al.[108] with permission.

(C) Reproduced from Shi et al.[110] with permission.

phenomena, of which notable examples include optical spin-hall effect[101] and controlled second harmonics radiation.[100]

Frustrated magnetic materials with QC architectures

Magnetism is usually generated through the coordination of magnetic spins, but, in the structures where spin coordination becomes impossible, special magnetism can be generated (i.e., spin frustration).[136,137] An example of spin frustration is spin ice, a material in which the magnetic spins act like iced water molecules (i.e., ice rule) without a single degenerated minimal energy state (Figure 8A).[136,137] QC-structured

magnetic materials, called magnetic quasicrystals, also do not allow spin orchestration due to the lack of structural periodicity, leading to magnetic frustrations.[138] The theoretical foundation of magnetic quasicrystals was established by Vedmedenko et al.[139] Through Monte Carlo simulation, the authors applied Ising antiferromagnet models to an Ammann-Beenker tiling structure, revealing that the superposition of geometric frustration with the quasiperiodic ordering led to a 3D noncollinear antiferromagnetic spin structure.[139] Parallel to such theoretical studies, experimental reports of magnetic quasicrystals such as Sc-Fe-Zn, R-Ag-In, and Yb-Au-Al were published, spurring several important discoveries, including magnetic topology and quantum critical states.[138]

In addition to frustration between magnetic spins at the atomic level, magnets with QC architectures can also experience macroscopic magnetic frustrations.[108–110] Farmer et al. fabricated permalloy-films with a 10-fold QC net pattern using electron beam lithography (Figure 8B, top left), and visualized the magnetization map using scanning electron microscopy equipped with polarization analysis (SEMPA; Figure 8B, top right and bottom left).[108] SEMPA measurements unveiled swirled order and frustration within the sublattices at the vertices of the magnetic QC net (Figure 8B, bottom right).[108] Shi et al. observed macrospin degeneracy in a 10-fold QC-ordered nanosized-magnetic array (Figure 8C).[110] The authors fabricated a Penrose tiling pattern made from permalloy and investigated the magnetic domains, especially the local magnetic configuration at the vertices.[110] Two types of magnetic degeneracy were identified: quasi-1D "skeleton" group (black arrows in the Figure 8C) and "flippable" clusters group (blue and red arrows in the Figure 8C).[110] As opposed to the quasi-1D skeleton group, which can span in the entire pattern and be ordered in a long-range manner,[110] the flippable clusters group can be further classified depending on the magnetic degeneracy (i.e., red arrows indicate 2-fold degeneracy, while blue arrows indicate 10-fold degeneracy). In addition, these magnetic tiles were topologically induced by magnetic frustrations caused by their QC architectures.[110] A deeper understanding of exotic magnetic topology emerging from geometrical frustration caused by QC aperiodicity should be expected through further research in this field.

Design and art with QC patterns

QC patterns are often used in arts,[140,141] designs,[142] and so forth,[143] offering not only eye-pleasing decorations but also practical functions. Interestingly, QC patterns were designed for exterior decorations of buildings at least 700 years before quasicrystals were discovered. Lu and Steinhardt studied the decoration on the exterior walls of Abbasid Al-Mustansiriyya Madrasa in Baghdad, Iraq, which exhibited a QC pattern called the Girih tiling (Figures 9A and 9B), and was built in the early thirteenth century.[140] The early QC pattern is not alone; several ancient architectures with QC decorations were later found in Sultan's Lodge, Ottoman Green Mosque in Busra, Turkey (1424), Darb-i Imam Shrine, Isfahan, Iran (1463), and Mausoleum of I'timad al-Daula in Agra, India (1622). In the modern time, QC decorations are still popular for architectural design and can be found all around the world, such as the Liberal Arts and Science building in the Education City campus at Doha, Qatar; Pilgrimage Church of Saint John of Nepomuk at Zelená hora, Czech Republic; and the Salesforce Transit Center in San Francisco United States (Figure 9C). Furthermore, Ajlouni discussed the practical advantages of QC order in buildings.[142] The report indicates that QC walls and roofs are expected to offer unique architectural acoustics, potentially leading to advanced buildings with a wide range of light and sound-based technologies.[142] QC patterns' aesthetic excellence inspired contemporary artists and designers, and various QC motifs have been widely used in artworks (Figure 9D) and daily products.

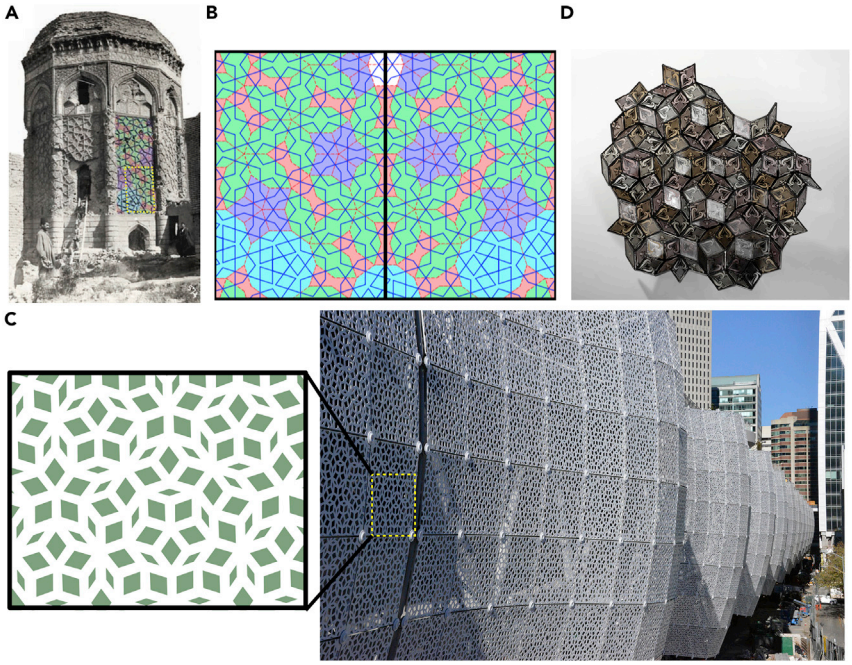

Figure 9. QC order found in architecture and art

(A) Photograph of the exterior walls of Abbasid Al-Mustansiriyya Madrasa in Baghdad, Iraq.

(B) QC order created through the Girih tiling that was found in the highlighted area in (A).

(C) Photograph of Salesforce Transit Center in San Francisco, United States.

(D) Baroque Quasicrystal by Debora Coombs.[141]

(A and B) Reproduced from Lu et al.,[140] with permission.

The photograph in (C) was taken by Peter Beeler, Metropolitan Transportation Commission and used with permission.

(D) Provided by Debora Coombs (https://www.coombscriddle.com/) and used with permission.

QC structure in unconventional dimensions

It is important to remember that patterns can be found not only in tangible spaces but also in other dimensions, such as time and electromagnetic fields. There have been inventions of patterned-in-unconventional-dimensions materials in recent years, such as optical lattices and time crystals, which we outline in this section.

QC optical lattices

Optical lattices consist of electromagnetic polarization patterns that are created through interference of multiple laser beams (Figure 10A, left). Optical lattices offer optical-trapping environments that are useful for research into particle physics such as Bose-Einstein condensate.[144–146] QC optical lattices are optical lattices with QC polarization patterns, which can provide distinct optical-trapping environments in which unnecessary interactions beyond optical traps can be minimized. QC optical lattices can serve as an indispensable study platform for understanding systems such as many-body localization and Bose glasses.[144,145] A theoretical foundation of QC optical lattices was created by the Santos' group,[144] who proposed using five laser beams placed pentagonally to generate a 5-fold symmetry QC optical lattice through interference. The first experimental demonstration of QC optical lattices was reported in 2019 by Viebahn et al.[145] The authors fabricated 8-fold QC optical lattices using four interfered laser beams and characterized them using raw time-of-flight images (Figure 10B),[145] which could successfully trap Bose-Einstein condensates of ^{39}K atoms.[145] Time-dependent diffraction measurements observed a continuous-time quantum walk (i.e., a quantum random walk from continuous-time

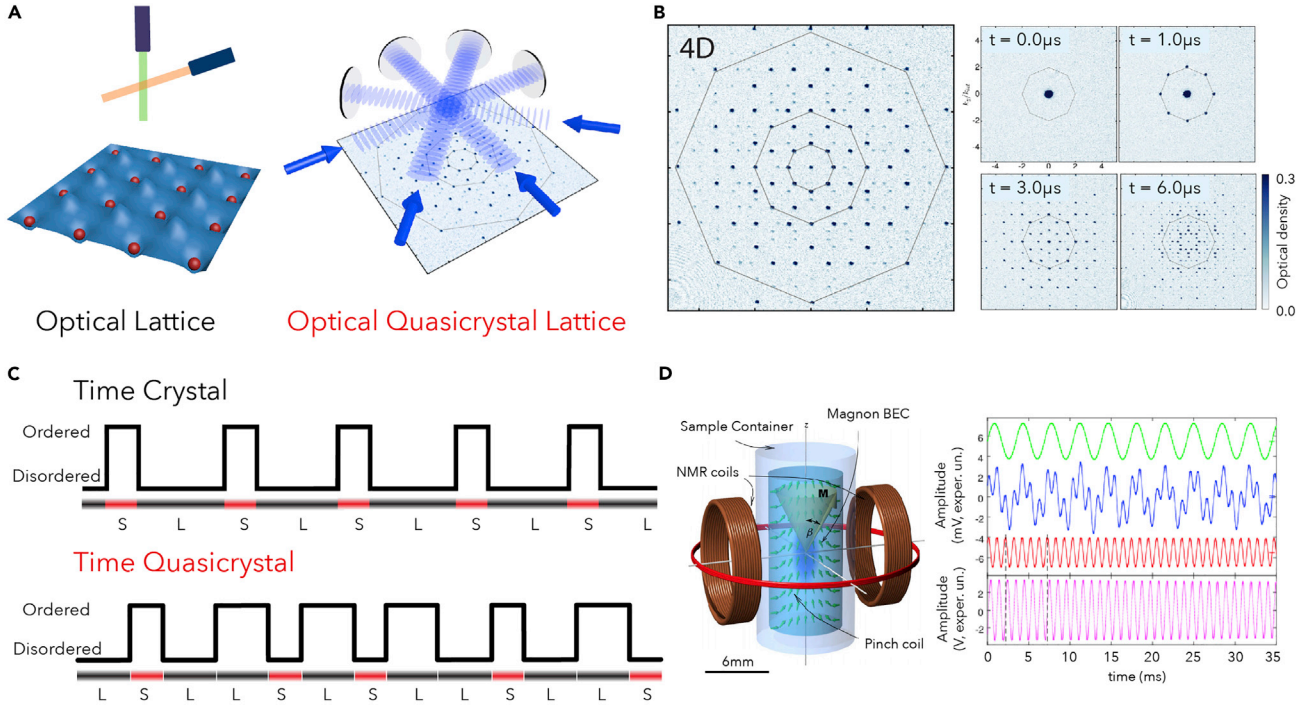

Figure 10. Optical QC lattices and time quasicrystals

(A) Schematics of (left) a conventional optical lattice and (right) an optical QC lattice.

(B) An 8-fold QC optical lattice. (Left) Time-of-flight image of the 8-fold QC optical lattices. (Right) Time-dependent Kapitza-Dirac diffraction patterns from the QC optical lattice.

(C) Schematics of (top) a time crystal and (bottom) a time quasicrystal.

(D) A discrete time quasicrystal created by Autti et al.[147] (Left) A setting to create time quasicrystals equipped with NMR coils and pinch coils; (right) QC signals from the time quasicrystal (blue line). The time QC was created under a periodic drive with an oscillating magnetic field (pink line), thus the QC signals (blue) of the time crystals were extracted from subtraction of the pink line from the original signal of the NMR coil. The signals from ground-level magnon Bose-Einstein condensate (BEC, green) and the (2,0) level (red) can be attributed to the QC signal (blue).

(B) Reproduced from Viebahn et al.,[145] with permission.

(D) Reproduced from Autti et al.,[147] with permission.

stochastic process) in a short time range, which had not been observed before.[145] Since QC structures possess unique local order, developing QC optical lattices with novel symmetry may serve as an important direction for future studies.

Time quasicrystals

The idea of time crystals, materials that repeat transformations without losing energy, was firstly conceptualized by Frank Wilczek in 2012.[148] As shown in Figure 10C top, time crystals can exhibit periodic oscillations between ordered and disordered states depending on the sequence of transformation processes. Wilczek predicted that such time crystals can only be possible in thermodynamic environments where an equilibrium state cannot be reached (i.e., non-equilibrium systems).[148] In 2017, two pioneering experimental works by Lukin et al.[149] and Monroe et al.[150] were simultaneously published. The materials used in these experiments were $^{171}Yb^{+}$ ions chain trapped in a linear radiofrequency Paul trap[150] and dipolar spin impurities from nitrogen-vacancies in a diamond.[149] In each experiment, oscillations between two hyperfine electron states and two spin states were observed under carefully designed conditions, respectively. After the initial discovery, in late 2021, researchers at Google, along with physicists in universities, demonstrated completely discrete time crystals using a quantum computer, eliminating the crucial instability problem.[151]

Despite the field still being in an early stage, researchers have already begun integrating QC order into time crystals (dubbed time quasicrystals).[147,152–154] Time quasicrystals exhibit oscillation between two states with a pattern following a 1D-QC order; e.g., Fibonacci sequence (Figure 10C, bottom). For example, Autti et al. used superfluid ^{3}He-B to demonstrate a time quasicrystal by applying magnetic fields that induce oscillations between two electronic spin configurations (i.e., magnon) (Figure 10D).[147] A frequency of coherent spin precession of ^{3}He-B was found to be incommensurate with the oscillating magnetic field, indicating that the discrete time translation symmetry broke spontaneously and hence time quasicrystals were confirmed.[147] Even though more work needs to be done to better understand time quasicrystals, e.g., the stability and the discreteness, time quasicrystals attracted a significant amount of attention from particle physics and astrophysics because they could serve as a steppingstone in connecting ordered and disordered states beyond conventional dimensions. This research topic crosses a wide range of disciplines, including fluctuation physics, gravitational theory, loop quantum gravity, and black hole formation.[155,156]

PERSPECTIVES

The paradigm shift caused by the discovery of quasicrystals has changed how researchers think about modern materials or matter in general. As we discussed in this review, substantial achievements have been made in the field of NA-QC materials and architectures, leveraging knowledge gained from atomic quasicrystal studies. However, compared with the knowledge base for crystalline structural matter, the field of QC materials is still in its infant stage. Keen efforts from diverse disciplines are undoubtedly needed to continuously advance this unique category of materials. Various aspects of QC materials research are still urgently needed. For example, production of stable and perfect NA-QC self-assemblies has not yet been convincingly demonstrated. Such effort is imperative since understanding of complete QC assemblies will not only enrich the library of QC materials but also lead to a comprehensive relationship among all structured matter from amorphous solids, to quasicrystals, to crystalline materials.[157] As another important aspect of QC research, in-depth understanding of the driving forces and formation dynamics for QC nucleation and growth in spontaneous assembly systems is mostly lacking. Rational design rules rather than random observations of such built QC systems have not yet been delineated. These fundamental limitations set inevitable hurdles toward further explorations of materials' properties and functionalities, and thus toward real-life application implementations of such QC assembled materials. On the bright side, such mechanistic studies, in principle, have recently become more feasible due to substantial advancements in materials fabrication methods and development of modern advanced characterization techniques with unprecedented spatial and temporal resolutions. More than ever, effective utilization of advanced characterization techniques has already been demonstrated with tremendous value for investigating the molecular and NC self-assembly systems with much greater detail in real time. State-of-the-art *in situ* high-resolution microscopies (e.g., TEM, atomic force microscopy [AFM])[46,158] and *in situ* synchrotron-based X-ray scattering/diffraction techniques are promising for future research.[159–161] Looking further ahead, exponential growth of computing power, fast development of simulation algorithms, and software implementing new crystallography techniques will promote further analytical advances that enable researchers to resolve sophisticated QC structure and explicate formation mechanisms at an unparalleled level.

For scientists, engineers, and designers who work on structure-property relationships, researching materials with QC order unquestionably serves as a fascinating topic as it provides immense opportunities, yet with unforeseeable challenges. Further progress in the field needs to be fueled by concerted efforts for advancing both experimental techniques and theoretical understanding. Discovery of atomic quasicrystals has forever changed the fundamental view of matter and shifted the paradigm of conventional structure recognition. Extrapolating such QC structures and patterns to materials and architectures made from non-atom building blocks crossing molecular scale, through nano- and meso-range to macroscopic objects, decoration patterns, and artwork designs will unleash phenomena and properties of matter that are even thought to be impossible today.

ACKNOWLEDGMENTS

O.C. acknowledges the support from National Science Foundation, United States through the CAREER grant (DMR-1943930). We also thank Debora Coombs (https://www.coombscriddle.com/) for generously providing her artwork.

AUTHOR CONTRIBUTIONS

Conceptualization, Y.N. and O.C.; writing, Y.N., H.Z., J.S., and O.C.; supervision, O.C.

DECLARATION OF INTERESTS

The authors declare no competing interests.

REFERENCES

1. Kleiner, I. (1986). The evolution of group theory: a brief survey. Math. Mag. *59*, 195–215.
2. Farkas, D.R. (1981). Crystallographic groups and their mathematics. Rocky. Mt. J. Math. *11*, 511–551. https://doi.org/10.1216/Rmj-1981-11-4-511.
3. Steurer, W. (2012). Fascinating quasicrystals. Chem. Soc. Rev. *41*, 6717–6718. https://doi.org/10.1039/c2cs90077g.
4. Shechtman, D., Blech, I., Gratias, D., and Cahn, J.W. (1984). Metallic phase with long-range orientational order and No translational symmetry. Phys. Rev. Lett. *53*, 1951–1953. https://doi.org/10.1103/PhysRevLett.53.1951.
5. Levine, D., and Steinhardt, P.J. (1984). Quasicrystals - a new class of ordered structures. Phys. Rev. Lett. *53*, 2477–2480. https://doi.org/10.1103/PhysRevLett.53.2477.
6. de Bruijn, N.G. (1986). Quasicrystals and their Fourier transform. Indagat. Math. *89*, 123–152.
7. Caspar, D.L., and Fontano, E. (1996). Five-fold symmetry in crystalline quasicrystal lattices. Proc. Natl. Acad. Sci. USA *93*, 14271–14278. https://doi.org/10.1073/pnas.93.25.14271.
8. Steurer, W. (2012). Why are quasicrystals quasiperiodic? Chem. Soc. Rev. *41*, 6719–6729. https://doi.org/10.1039/c2cs35063g.
9. Janssen, T., and Janner, A. (2014). Aperiodic crystals and superspace concepts. Acta Crystallogr. B Struct. Sci. Cryst. Eng. Mater. *70*, 617–651. https://doi.org/10.1107/S2052520614014917.
10. Li, R.T., Li, Z., Dong, Z.L., and Khor, K.A. (2016). A review of transmission electron microscopy of quasicrystals-how are atoms arranged? Crystals *6*, 105.
11. International Union of Crystallography - Report of the Executive-Committee for 1991 (1992). Acta Crystallogr. A *48*, 922–946.
12. Young Park, J., Ogletree, D.F., Salmeron, M., Ribeiro, R.A., Canfield, P.C., Jenks, C.J., and Thiel, P.A. (2006). Tribological properties of quasicrystals: effect of aperiodic versus periodic surface order. Phys. Rev. B *74*, 024203.
13. Louzguine-Luzgin, D.V., and Inoue, A. (2008). Formation and properties of quasicrystals. Annu. Rev. Mater. Res. *38*, 403–423. https://doi.org/10.1146/annurev.38.060407.130318.
14. Dubois, J.M. (2012). Properties- and applications of quasicrystals and complex metallic alloys. Chem. Soc. Rev. *41*, 6760–6777. https://doi.org/10.1039/c2cs35110b.
15. Tsai, A.P. (2013). Discovery of stable icosahedral quasicrystals: progress in understanding structure and properties. Chem. Soc. Rev. *42*, 5352–5365. https://doi.org/10.1039/c3cs35388e.
16. Yamamoto, A. (1996). Crystallography of quasiperiodic crystals. Acta Crystallogr. A *52*, 509–560. https://doi.org/10.1107/S0108767396000967.
17. Lifshitz, R. (2003). A matter of definition. Found. Phys. *33*, 1703–1711. https://doi.org/10.1023/A:1026247120031.
18. Abe, E. (2012). Electron microscopy of quasicrystals - where are the atoms? Chem. Soc. Rev. *41*, 6787–6798. https://doi.org/10.1039/c2cs35303b.
19. Steurer, W. (2018). What do we know? What do we want to know? What can we know? Acta Crystallogr. A Found. Adv. *74*, 1–11. https://doi.org/10.1107/S2053273317016540.
20. Stadnik, Z.M. (1999). Physical Properties of Quasicrystals (Springer).
21. Steurer, W., and Deloudi, S. (2009). Crystallography of Quasicrystals: Concepts, Methods and Structures (Springer Heidelberg).
22. Nagaoka, Y., Zhu, H., Eggert, D., and Chen, O. (2018). Single-component quasicrystalline nanocrystal superlattices through flexible polygon tiling rule. Science *362*, 1396–1400. https://doi.org/10.1126/science.aav0790.
23. Goodman-Strauss, C. (1998). Matching rules and substitution tilings. Ann. Math. *147*, 181–223. https://doi.org/10.2307/120988.
24. Goodman-Strauss, C. (2018). Lots of aperiodic sets of tiles. J. Combin. Theor. *160*, 409–445. https://doi.org/10.1016/j.jcta.2018.07.002.
25. Wang, N., Chen, H., and Kuo, K.H. (1987). Two-dimensional quasicrystal with eightfold rotational symmetry. Phys. Rev. Lett. *59*,

1010–1013. https://doi.org/10.1103/PhysRevLett.59.1010.

26. Steurer, W. (2004). Twenty years of structure research on quasicrystals. Part 1. Pentagonal, octagonal, decagonal and dodecagonal quasicrystals. Z. Kristallogr. *219*, 391–446. https://doi.org/10.1524/zkri.219.7.391.35643.

27. Grünbaum, B., and Shephard, G.C. (2016). Tilings and Patterns, Second edition (Dover Publications, Inc).

28. Taniguchi, S., and Abe, E. (2008). Highly-perfect decagonal quasicrystalline Al(64) Cu(22)Co(14) with non-centrosymmetry. Phil. Mag. *88*, 1949–1958. https://doi.org/10.1080/14786430802035683.

29. Conrad, M., Krumeich, F., and Harbrecht, B. (1998). A dodecagonal quasicrystalline chalcogenide. Angew Chem. Int. Ed. Engl. *37*, 1383–1386.

30. Man, W., Megens, M., Steinhardt, P.J., and Chaikin, P.M. (2005). Experimental measurement of the photonic properties of icosahedral quasicrystals. Nature *436*, 993–996. https://doi.org/10.1038/nature03977.

31. Jeong, H.C., and Steinhardt, P.J. (1994). Cluster approach for quasicrystals. Phys. Rev. Lett. *73*, 1943–1946. https://doi.org/10.1103/PhysRevLett.73.1943.

32. Nakakura, J., Ziherl, P., Matsuzawa, J., and Dotera, T. (2019). Metallic-mean quasicrystals as aperiodic approximants of periodic crystals. Nat. Commun. *10*, 4235. https://doi.org/10.1038/s41467-019-12147-z.

33. Iacovella, C.R., Keys, A.S., and Glotzer, S.C. (2011). Self-assembly of soft-matter quasicrystals and their approximants. Proc. Natl. Acad. Sci. USA *108*, 20935–20940. https://doi.org/10.1073/pnas.1019763108.

34. Lindquist, B.A., Jadrich, R.B., Piñeros, W.D., and Truskett, T.M. (2018). Inverse design of self-assembling frank-kasper phases and insights into emergent quasicrystals. J. Phys. Chem. B *122*, 5547–5556. https://doi.org/10.1021/acs.jpcb.7b11841.

35. Yang, W., Feuerbacher, M., Tamura, N., Ding, D.H., Wang, R., and Urban, K. (1998). Atomic model of dislocations in Al-Pd-Mn icosahedral quasicrystals. Philos. Mag. A *77*, 1481–1497.

36. Fisher, I.R., Islam, Z., Panchula, A.F., Cheon, K.O., Kramer, M.J., Canfield, P.C., and Goldman, A.I. (1998). Growth of large-grain R-Mg-Zn quasicrystals from the ternary melt (R = Y, Er, Ho, Dy, Tb). Phil. Mag. B *77*, 1601–1615. https://doi.org/10.1080/13642819808206407.

37. Abe, E., Yan, Y., and Pennycook, S.J. (2004). Quasicrystals as cluster aggregates. Nat. Mater. *3*, 759–767. https://doi.org/10.1038/nmat1244.

38. Socolar, J.E., and Steinhardt, P.J. (1986). Quasicrystals. II. Unit-cell configurations. Phys. Rev. B Condens. Matter *34*, 617–647. https://doi.org/10.1103/physrevb.34.617.

39. Hann, C.T., Socolar, J.E.S., and Steinhardt, P.J. (2016). Local growth of icosahedral quasicrystalline tilings. Phys. Rev. B *94*, 014113.

40. Madison, A.E. (2015). Substitution rules for icosahedral quasicrystals. RSC Adv. *5*, 5745–5753. https://doi.org/10.1039/c4ra09524c.

41. Talapin, D.V., Shevchenko, E.V., Bodnarchuk, M.I., Ye, X., Chen, J., and Murray, C.B. (2009). Quasicrystalline order in self-assembled binary nanoparticle superlattices. Nature *461*, 964–967. https://doi.org/10.1038/nature08439.

42. Bodnarchuk, M.I., Shevchenko, E.V., and Talapin, D.V. (2011). Structural defects in periodic and quasicrystalline binary nanocrystal superlattices. J. Am. Chem. Soc. *133*, 20837–20849. https://doi.org/10.1021/ja207154v.

43. Yang, Z., Wei, J., Bonville, P., and Pileni, M.P. (2015). Beyond entropy: magnetic forces induce formation of quasicrystalline structure in binary nanocrystal superlattices. J. Am. Chem. Soc. *137*, 4487–4493. https://doi.org/10.1021/jacs.5b00332.

44. Bodnarchuk, M.I., Erni, R., Krumeich, F., and Kovalenko, M.V. (2013). Binary superlattices from colloidal nanocrystals and giant polyoxometalate clusters. Nano Lett. *13*, 1699–1705. https://doi.org/10.1021/nl4002475.

45. Ye, X., Chen, J., Eric Irrgang, M., Engel, M., Dong, A., Glotzer, S.C., and Murray, C.B. (2017). Quasicrystalline nanocrystal superlattice with partial matching rules. Nat. Mater. *16*, 214–219. https://doi.org/10.1038/Nmat4759.

46. Nagaoka, Y., Tan, R., Li, R., Zhu, H., Eggert, D., Wu, Y.A., Liu, Y., Wang, Z., and Chen, O. (2018). Superstructures generated from truncated tetrahedral quantum dots. Nature *561*, 378–382. https://doi.org/10.1038/s41586-018-0512-5.

47. Wasio, N.A., Quardokus, R.C., Forrest, R.P., Lent, C.S., Corcelli, S.A., Christie, J.A., Henderson, K.W., and Kandel, S.A. (2014). Self-assembly of hydrogen-bonded two-dimensional quasicrystals. Nature *507*, 86–89. https://doi.org/10.1038/nature12993.

48. Brown, R.D., Corcelli, S.A., and Kandel, S.A. (2018). Structural polymorphism as the result of kinetically controlled self-assembly. Acc. Chem. Res. *51*, 465–474. https://doi.org/10.1021/acs.accounts.7b00522.

49. Urgel, J.I., Écija, D., Lyu, G., Zhang, R., Palma, C.A., Auwärter, W., Lin, N., and Barth, J.V. (2016). Quasicrystallinity expressed in two-dimensional coordination networks. Nat. Chem. *8*, 657–662. https://doi.org/10.1038/nchem.2507.

50. Sun, Y., Ma, K., Kao, T., Spoth, K.A., Sai, H., Zhang, D., Kourkoutis, L.F., Elser, V., and Wiesner, U. (2017). Formation pathways of mesoporous silica nanoparticles with dodecagonal tiling. Nat. Commun. *8*, 252. https://doi.org/10.1038/s41467-017-00351-8.

51. Zhang, Y.Q., Paszkiewicz, M., Du, P., Zhang, L., Lin, T., Chen, Z., Klyatskaya, S., Ruben, M., Seitsonen, A.P., Barth, J.V., and Klappenberger, F. (2018). Complex supramolecular interfacial tessellation through convergent multi-step reaction of a dissymmetric simple organic precursor. Nat. Chem. *10*, 296–304. https://doi.org/10.1038/Nchem.2924.

52. Xiao, C., Fujita, N., Miyasaka, K., Sakamoto, Y., and Terasaki, O. (2012). Dodecagonal tiling in mesoporous silica. Nature *487*, 349–353. https://doi.org/10.1038/nature11230.

53. Zeng, X., Ungar, G., Liu, Y., Percec, V., Dulcey, A.E., and Hobbs, J.K. (2004). Supramolecular dendritic liquid quasicrystals. Nature *428*, 157–160. https://doi.org/10.1038/nature02368.

54. Yue, K., Huang, M., Marson, R.L., He, J., Huang, J., Zhou, Z., Wang, J., Liu, C., Yan, X., Wu, K., et al. (2016). Geometry induced sequence of nanoscale Frank-Kasper and quasicrystal mesophases in giant surfactants. Proc. Natl. Acad. Sci. USA *113*, 14195–14200. https://doi.org/10.1073/pnas.1609422113.

55. Holerca, M.N., Sahoo, D., Partridge, B.E., Peterca, M., Zeng, X., Ungar, G., and Percec, V. (2018). Dendronized poly(2-oxazoline) displays within only five monomer repeat units liquid quasicrystal, A15 and sigma frank-kasper phases. J. Am. Chem. Soc. *140*, 16941–16947. https://doi.org/10.1021/jacs.8b11103.

56. Feng, X., Liu, G., Guo, D., Lang, K., Zhang, R., Huang, J., Su, Z., Li, Y., Huang, M., Li, T., and Cheng, S.Z.D. (2019). Transition kinetics of self-assembled supramolecular dodecagonal quasicrystal and frank-kasper sigma phases in AB(n) dendron-like giant molecules. ACS Macro Lett. *8*, 875–881. https://doi.org/10.1021/acsmacrolett.9b00287.

57. Jayaraman, A., Baez-Cotto, C.M., Mann, T.J., and Mahanthappa, M.K. (2021). Dodecagonal quasicrystals of oil-swollen ionic surfactant micelles. Proc. Natl. Acad. Sci. USA *118*. e2101598118. https://doi.org/10.1073/pnas.2101598118.

58. Zhang, J., and Bates, F.S. (2012). Dodecagonal quasicrystalline morphology in a poly(styrene-b-isoprene-b-styrene-b-ethylene oxide) tetrablock terpolymer. J. Am. Chem. Soc. *134*, 7636–7639. https://doi.org/10.1021/ja301770v.

59. Hayashida, K., Dotera, T., Takano, A., and Matsushita, Y. (2007). Polymeric quasicrystal: mesoscopic quasicrystalline tiling in ABC star polymers. Phys. Rev. Lett. *98*. https://doi.org/10.1103/PhysRevLett.98.195502.

60. Miyamori, Y., Suzuki, J., Takano, A., and Matsushita, Y. (2020). Periodic and aperiodic tiling patterns from a tetrablock terpolymer system of the A(1)BA(2)C type. ACS Macro Lett. *9*, 32–37. https://doi.org/10.1021/acsmacrolett.9b00861.

61. Liu, L., Li, Z., Li, Y., and Mao, C. (2019). Rational design and self-assembly of two-dimensional, dodecagonal DNA quasicrystals. J. Am. Chem. Soc. *141*, 4248–4251. https://doi.org/10.1021/jacs.9b00843.

62. Whitesides, G.M., and Grzybowski, B. (2002). Self-assembly at all scales. Science *295*, 2418–2421. https://doi.org/10.1126/science.1070821.

63. Murray, C.B., Kagan, C.R., and Bawendi, M.G. (2000). Synthesis and characterization of monodisperse nanocrystals and close-packed

nanocrystal assemblies. Annu. Rev. Mater. Sci. *30*, 545–610. https://doi.org/10.1146/annurev.matsci.30.1.545.

64. Tan, R., Zhu, H., Cao, C., and Chen, O. (2016). Multi-component superstructures self-assembled from nanocrystal building blocks. Nanoscale *8*, 9944–9961. https://doi.org/10.1039/c6nr01662f.

65. Boles, M.A., Engel, M., and Talapin, D.V. (2016). Self-assembly of colloidal nanocrystals: from intricate structures to functional materials. Chem. Rev. *116*, 11220–11289. https://doi.org/10.1021/acs.chemrev.6b00196.

66. Deng, K., Luo, Z., Tan, L., and Quan, Z. (2020). Self-assembly of anisotropic nanoparticles into functional superstructures. Chem. Soc. Rev. *49*, 6002–6038. https://doi.org/10.1039/d0cs00541j.

67. Nagaoka, Y., Chen, O., Wang, Z., and Cao, Y.C. (2012). Structural control of nanocrystal superlattices using organic guest molecules. J. Am. Chem. Soc. *134*, 2868–2871. https://doi.org/10.1021/ja209062d.

68. Nagaoka, Y., Hills-Kimball, K., Tan, R., Li, R., Wang, Z., and Chen, O. (2017). Nanocube superlattices of cesium lead bromide perovskites and pressure-induced phase transformations at atomic and mesoscale levels. Adv. Mater. *29*, 1606666. https://doi.org/10.1002/adma.201606666.

69. Zhu, H., Nagaoka, Y., Hills-Kimball, K., Tan, R., Yu, L., Fang, Y., Wang, K., Li, R., Wang, Z., and Chen, O. (2017). Pressure-enabled synthesis of hetero-dimers and hetero-rods through intraparticle coalescence and interparticle fusion of quantum-dot-Au satellite nanocrystals. J. Am. Chem. Soc. *139*, 8408–8411. https://doi.org/10.1021/jacs.7b04018.

70. Zhu, H., Fan, Z., Yu, L., Wilson, M.A., Nagaoka, Y., Eggert, D., Cao, C., Liu, Y., Wei, Z., Wang, X., et al. (2019). Controlling nanoparticle orientations in the self-assembly of patchy quantum dot-gold heterostructural nanocrystals. J. Am. Chem. Soc. *141*, 6013–6021. https://doi.org/10.1021/jacs.9b01033.

71. Cherniukh, I., Rainò, G., Stöferle, T., Burian, M., Travesset, A., Naumenko, D., Amenitsch, H., Erni, R., Mahrt, R.F., Bodnarchuk, M.I., and Kovalenko, M.V. (2021). Perovskite-type superlattices from lead halide perovskite nanocubes. Nature *593*, 535–542. https://doi.org/10.1038/s41586-021-03492-5.

72. Shevchenko, E.V., Talapin, D.V., Kotov, N.A., O'Brien, S., and Murray, C.B. (2006). Structural diversity in binary nanoparticle superlattices. Nature *439*, 55–59. https://doi.org/10.1038/nature04414.

73. Lin, H., Lee, S., Sun, L., Spellings, M., Engel, M., Glotzer, S.C., and Mirkin, C.A. (2017). Clathrate colloidal crystals. Science *355*, 931–935. https://doi.org/10.1126/science.aal3919.

74. Wang, D., Dasgupta, T., van der Wee, E.B., Zanaga, D., Altantzis, T., Wu, Y., Coli, G.M., Murray, C.B., Bals, S., Dijkstra, M., and van Blaaderen, A. (2021). Binary icosahedral clusters of hard spheres in spherical confinement. Nat. Phys. *17*, 128–134. https://doi.org/10.1038/s41567-020-1003-9.

75. Noya, E.G., Wong, C.K., Llombart, P., and Doye, J.P.K. (2021). How to design an icosahedral quasicrystal through directional bonding. Nature *596*, 367–371. https://doi.org/10.1038/s41586-021-03700-2.

76. Damasceno, P.F., Engel, M., and Glotzer, S.C. (2012). Predictive self-assembly of polyhedra into complex structures. Science *337*, 453–457. https://doi.org/10.1126/science.1220869.

77. Haji-Akbari, A., Engel, M., Keys, A.S., Zheng, X., Petschek, R.G., Palffy-Muhoray, P., and Glotzer, S.C. (2009). Disordered, quasicrystalline and crystalline phases of densely packed tetrahedra. Nature *462*, 773–777. https://doi.org/10.1038/nature08641.

78. Chen, E.R., Engel, M., and Glotzer, S.C. (2010). Dense crystalline dimer packings of regular tetrahedra. Discrete Comput. Geom. *44*, 253–280. https://doi.org/10.1007/s00454-010-9273-0.

79. Conway, J.H., and Torquato, S. (2006). Packing, tiling, and covering with tetrahedra. Proc. Natl. Acad. Sci. USA *103*, 10612–10617. https://doi.org/10.1073/pnas.0601389103.

80. Yin, J.S., and Wang, Z.L. (1997). Ordered self-assembling of tetrahedral oxide nanocrystals. Phys. Rev. Lett. *79*, 2570–2573. https://doi.org/10.1103/PhysRevLett.79.2570.

81. Tang, Z., Zhang, Z., Wang, Y., Glotzer, S.C., and Kotov, N.A. (2006). Self-assembly of CdTe nanocrystals into free-floating sheets. Science *314*, 274–278. https://doi.org/10.1126/science.1128045.

82. Niu, Z., Peng, Q., Gong, M., Rong, H., and Li, Y. (2011). Oleylamine-mediated shape evolution of palladium nanocrystals. Angew Chem. Int. Ed. Engl. *50*, 6315–6319. https://doi.org/10.1002/anie.201100512.

83. Zola, R.S., Bisoyi, H.K., Wang, H., Urbas, A.M., Bunning, T.J., and Li, Q. (2019). Dynamic control of light direction enabled by stimuli-responsive liquid crystal gratings. Adv. Mater. *31*, e1806172. https://doi.org/10.1002/adma.201806172.

84. Förster, S., Meinel, K., Hammer, R., Trautmann, M., and Widdra, W. (2013). Quasicrystalline structure formation in a classical crystalline thin-film system. Nature *502*, 215–218. https://doi.org/10.1038/nature12514.

85. Chanpuriya, S., Kim, K., Zhang, J., Lee, S., Arora, A., Dorfman, K.D., Delaney, K.T., Fredrickson, G.H., and Bates, F.S. (2016). Cornucopia of nanoscale ordered phases in sphere-forming tetrablock terpolymers. ACS Nano *10*, 4961–4972. https://doi.org/10.1021/acsnano.6b00495.

86. Maciá, E. (2006). The role of aperiodic order in science and technology. Rep. Prog. Phys. *69*, 397–441. https://doi.org/10.1088/0034-4885/69/2/R03.

87. de Boissieu, M. (2012). Phonons, phasons and atomic dynamics in quasicrystals. Chem. Soc. Rev. *41*, 6778–6786. https://doi.org/10.1039/c2cs35212e.

88. Ishimasa, T., Iwami, S., Sakaguchi, N., Oota, R., and Mihalkovič, M. (2015). Phason space analysis and structure modelling of 100 angstrom-scale dodecagonal quasicrystal in Mn-based alloy. Phil. Mag. *95*, 3745–3767. https://doi.org/10.1080/14786435.2015.1095365.

89. Engel, M., and Trebin, H.R. (2007). Self-assembly of monatomic complex crystals and quasicrystals with a double-well interaction potential. Phys. Rev. Lett. *98*, 225505. https://doi.org/10.1103/PhysRevLett.98.225505.

90. Achim, C.V., Schmiedeberg, M., and Löwen, H. (2014). Growth modes of quasicrystals. Phys. Rev. Lett. *112*, 255501. https://doi.org/10.1103/PhysRevLett.112.255501.

91. Nagao, K., Inuzuka, T., Nishimoto, K., and Edagawa, K. (2015). Experimental observation of quasicrystal growth. Phys. Rev. Lett. *115*, 075501. https://doi.org/10.1103/PhysRevLett.115.075501.

92. Han, I., Wang, K.L., Cadotte, A.T., Xi, Z., Parsamehr, H., Xiao, X., Glotzer, S.C., and Shahani, A.J. (2021). Formation of a single quasicrystal upon collision of multiple grains. Nat. Commun. *12*, 5790. https://doi.org/10.1038/s41467-021-26070-9.

93. Keys, A.S., and Glotzer, S.C. (2007). How do quasicrystals grow? Phys. Rev. Lett. *99*, 235503. https://doi.org/10.1103/PhysRevLett.99.235503.

94. Jiang, Z., Quan, S., Xu, N., He, L., and Ni, Y. (2020). Growth modes of quasicrystals involving intermediate phases and a multistep behavior studied by phase field crystal model. Phys. Rev. Mater. *4*, 023403. https://doi.org/10.1103/PhysRevMaterials.4.023403.

95. De Yoreo, J.J., Gilbert, P.U.P.A., Sommerdijk, N.A.J.M., Penn, R.L., Whitelam, S., Joester, D., Zhang, H., Rimer, J.D., Navrotsky, A., Banfield, J.F., et al. (2015). Crystallization by particle attachment in synthetic, biogenic, and geologic environments. Science *349*. https://doi.org/10.1126/science.aaa6760.

96. Grzybowski, B.A., Fitzner, K., Paczesny, J., and Granick, S. (2017). From dynamic self-assembly to networked chemical systems. Chem. Soc. Rev. *46*, 5647–5678. https://doi.org/10.1039/c7cs00089h.

97. Vardeny, Z.V., Nahata, A., and Agrawal, A. (2013). Optics of photonic quasicrystals. Nat. Photonics *7*, 177–187. https://doi.org/10.1038/Nphoton.2012.343.

98. Maciá, E. (2012). Exploiting aperiodic designs in nanophotonic devices. Rep. Prog. Phys. *75*, 036502. https://doi.org/10.1088/0034-4885/75/3/036502.

99. Kruk, S.S., Helgert, C., Decker, M., Staude, I., Menzel, C., Etrich, C., Rockstuhl, C., Jagadish, C., Pertsch, T., Neshev, D.N., and Kivshar, Y.S. (2013). Optical metamaterials with quasicrystalline symmetry: symmetry-induced optical isotropy. Phys. Rev. B *88*, 201404. https://doi.org/10.1103/PhysRevB.88.201404.

100. Tang, Y., Deng, J., Li, K.F., Jin, M., Ng, J., and Li, G. (2019). Quasicrystal photonic metasurfaces for radiation controlling of second harmonic generation. Adv. Mater. *31*, e1901188. https://doi.org/10.1002/adma.201901188.

101. Yulevich, I., Maguid, E., Shitrit, N., Veksler, D., Kleiner, V., and Hasman, E. (2015). Optical mode control by geometric phase in quasicrystal metasurface. Phys. Rev. Lett. *115*, 205501. https://doi.org/10.1103/PhysRevLett.115.205501.

102. Yang, Q., Zhang, X., Li, S., Xu, Q., Singh, R., Liu, Y., Li, Y., Kruk, S.S., Gu, J., Han, J., and Zhang, W. (2016). Near-field surface plasmons on quasicrystal metasurfaces. Sci. Rep. *6*, 26. https://doi.org/10.1038/s41598-016-0027-y.

103. Dontabhaktuni, J., Ravnik, M., and Zumer, S. (2018). Quasicrystalline ordering in thin liquid crystal films. Crystals *8*, 275. https://doi.org/10.3390/cryst8070275.

104. Mikhael, J., Roth, J., Helden, L., and Bechinger, C. (2008). Archimedean-like tiling on decagonal quasicrystalline surfaces. Nature *454*, 501–504. https://doi.org/10.1038/nature07074.

105. Notomi, M., Suzuki, H., Tamamura, T., and Edagawa, K. (2004). Lasing action due to the two-dimensional quasiperiodicity of photonic quasicrystals with a Penrose lattice. Phys. Rev. Lett. *92*, 123906. https://doi.org/10.1103/PhysRevLett.92.123906.

106. Noda, S., Yokoyama, M., Imada, M., Chutinan, A., and Mochizuki, M. (2001). Polarization mode control of two-dimensional photonic crystal laser by unit cell structure design. Science *293*, 1123–1125. https://doi.org/10.1126/science.1061738.

107. Mahler, L., Tredicucci, A., Beltram, F., Walther, C., Faist, J., Beere, H.E., Ritchie, D.A., and Wiersma, D.S. (2010). Quasi-periodic distributed feedback laser. Nat. Photonics *4*, 165–169. https://doi.org/10.1038/Nphoton.2009.285.

108. Farmer, B., Bhat, V.S., Balk, A., Teipel, E., Smith, N., Unguris, J., Keavney, D.J., Hastings, J.T., and De Long, L.E. (2016). Direct imaging of coexisting ordered and frustrated sublattices in artificial ferromagnetic quasicrystals. Phys. Rev. B *93*, 134428. https://doi.org/10.1103/PhysRevB.93.134428.

109. Brajuskovic, V., Barrows, F., Phatak, C., and Petford-Long, A.K. (2016). Real-space observation of magnetic excitations and avalanche behavior in artificial quasicrystal lattices. Sci. Rep. *6*, 34384. https://doi.org/10.1038/srep34384.

110. Shi, D., Budrikis, Z., Stein, A., Morley, S.A., Olmsted, P.D., Burnell, G., and Marrows, C.H. (2018). Frustration and thermalization in an artificial magnetic quasicrystal. Nat. Phys. *14*, 309–314. https://doi.org/10.1038/s41567-017-0009-4.

111. Pierce, F.S., Poon, S.J., and Guo, Q. (1993). Electron localization in metallic quasicrystals. Science *261*, 737–739. https://doi.org/10.1126/science.261.5122.737.

112. Pope, A.L., Tritt, T.M., Chernikov, M.A., and Feuerbacher, M. (1999). Thermal and electrical transport properties of the single-phase quasicrystalline material: Al70.8Pd20.9Mn8.3. Appl. Phys. Lett. *75*, 1854–1856. https://doi.org/10.1063/1.124850.

113. Kamiya, K., Takeuchi, T., Kabeya, N., Wada, N., Ishimasa, T., Ochiai, A., Deguchi, K., Imura, K., and Sato, N.K. (2018). Discovery of superconductivity in quasicrystal. Nat. Commun. *9*, 154. https://doi.org/10.1038/s41467-017-02667-x.

114. Zoorob, M.E., Charlton, M.D.B., Parker, G.J., Baumberg, J.J., and Netti, M.C. (2000). Complete photonic bandgaps in 12-fold symmetric quasicrystals. Nature *404*, 740–743.

115. Gellermann, W., Kohmoto, M., Sutherland, B., and Taylor, P.C. (1994). Localization of light waves in Fibonacci dielectric multilayers. Phys. Rev. Lett. *72*, 633–636. https://doi.org/10.1103/PhysRevLett.72.633.

116. Kohmoto, M., Sutherland, B., and Iguchi, K. (1987). Localization of optics: quasiperiodic media. Phys. Rev. Lett. *58*, 2436–2438. https://doi.org/10.1103/PhysRevLett.58.2436.

117. Poddubny, A.N., Pilozzi, L., Voronov, M.M., and Ivchenko, E.L. (2008). Resonant Fibonacci quantum well structures in one dimension. Phys. Rev. B *77*, 113306. https://doi.org/10.1103/PhysRevB.77.113306.

118. Bellingeri, M., Chiasera, A., Kriegel, I., and Scotognella, F. (2017). Optical properties of periodic, quasi-periodic, and disordered one-dimensional photonic structures. Opt. Mater. *72*, 403–421. https://doi.org/10.1016/j.optmat.2017.06.033.

119. Freedman, B., Bartal, G., Segev, M., Lifshitz, R., Christodoulides, D.N., and Fleischer, J.W. (2006). Wave and defect dynamics in nonlinear photonic quasicrystals. Nature *440*, 1166–1169. https://doi.org/10.1038/nature04722.

120. Matsui, T., Agrawal, A., Nahata, A., and Vardeny, Z.V. (2007). Transmission resonances through aperiodic arrays of subwavelength apertures. Nature *446*, 517–521. https://doi.org/10.1038/nature05620.

121. Florescu, M., Torquato, S., and Steinhardt, P.J. (2009). Complete band gaps in two-dimensional photonic quasicrystals. Phys. Rev. B *80*, 155112. https://doi.org/10.1103/PhysRevB.80.155112.

122. Thon, S.M., Irvine, W.T.M., Kleckner, D., and Bouwmeester, D. (2010). Polychromatic photonic quasicrystal cavities. Phys. Rev. Lett. *104*, 243901. https://doi.org/10.1103/PhysRevLett.104.243901.

123. Levi, L., Rechtsman, M., Freedman, B., Schwartz, T., Manela, O., and Segev, M. (2011). Disorder-enhanced transport in photonic quasicrystals. Science *332*, 1541–1544. https://doi.org/10.1126/science.1202977.

124. Ledermann, A., Cademartiri, L., Hermatschweiler, M., Toninelli, C., Ozin, G.A., Wiersma, D.S., Wegener, M., and von Freymann, G. (2006). Three-dimensional silicon inverse photonic quasicrystals for infrared wavelengths. Nat. Mater. *5*, 942–945. https://doi.org/10.1038/nmat1786.

125. Sinelnik, A.D., Shishkin, I.I., Yu, X., Samusev, K.B., Belov, P.A., Limonov, M.F., Ginzburg, P., and Rybin, M.V. (2020). Experimental observation of intrinsic light localization in photonic icosahedral quasicrystals. Adv. Opt. Mater. *8*, 2001170. https://doi.org/10.1002/adom.202001170.

126. Kalish, A.N., Komarov, R.S., Kozhaev, M.A., Achanta, V.G., Dagesyan, S.A., Shaposhnikov, A.N., Prokopov, A.R., Berzhansky, V.N., Zvezdin, A.K., and Belotelov, V.I. (2018). Magnetoplasmonic quasicrystals: an approach for multiband magneto-optical response. Optica *5*, 617–623. https://doi.org/10.1364/Optica.5.000617.

127. Gopinath, A., Boriskina, S.V., Feng, N.N., Reinhard, B.M., and Dal Negro, L. (2008). Photonic-plasmonic scattering resonances in deterministic aperiodic structures. Nano Lett. *8*, 2423–2431. https://doi.org/10.1021/nl8013692.

128. Lee, S.Y., Amsden, J.J., Boriskina, S.V., Gopinath, A., Mitropolous, A., Kaplan, D.L., Omenetto, F.G., and Dal Negro, L. (2010). Spatial and spectral detection of protein monolayers with deterministic aperiodic arrays of metal nanoparticles. Proc. Natl. Acad. Sci. USA *107*, 12086–12090. https://doi.org/10.1073/pnas.1002849107.

129. Ravishankar, A.P., Yallapragada, V.J., Kasture, S., Nagarajan, A., and Achanta, V.G. (2016). Broadband linear and nonlinear optical response of plasmonic quasicrystals. Opt Commun. *366*, 57–60. https://doi.org/10.1016/j.optcom.2015.12.032.

130. Achanta, V.G. (2015). Plasmonic quasicrystals. Prog. Quant. Electron. *39*, 1–23. https://doi.org/10.1016/j.pquantelec.2014.12.002.

131. Soukoulis, C.M., and Wegener, M. (2011). Past achievements and future challenges in the development of three-dimensional photonic metamaterials. Nat. Photonics *5*, 523–530. https://doi.org/10.1038/Nphoton.2011.154.

132. Kildishev, A.V., Boltasseva, A., and Shalaev, V.M. (2013). Planar photonics with metasurfaces. Science *339*, 1232009. https://doi.org/10.1126/science.1232009.

133. Khorasaninejad, M., and Capasso, F. (2017). Metalenses: versatile multifunctional photonic components. Science *358*. https://doi.org/10.1126/science.aam8100.

134. Roichman, Y., and Grier, D. (2005). Holographic assembly of quasicrystalline photonic heterostructures. Opt Express *13*, 5434–5439. https://doi.org/10.1364/Opex.13.005434.

135. Ovanesyan, Z., Pudasaini, P.R., Gangadharan, A., and Marucho, M. (2013). Three-dimensional quasicrystalline photonic material with five-fold planar symmetry for visible and infrared wavelengths by holographic assembly of quasicrystalline photonic heterostructures. Opt. Mater. Express *3*, 1332–1337. https://doi.org/10.1364/Ome.3.001332.

136. Fennell, T., Deen, P.P., Wildes, A.R., Schmalzl, K., Prabhakaran, D., Boothroyd, A.T., Aldus, R.J., McMorrow, D.F., and Bramwell, S.T. (2009). Magnetic Coulomb phase in the spin ice Ho2Ti2O7. Science *326*, 415–417. https://doi.org/10.1126/science.1177582.

137. Morris, D.J.P., Tennant, D.A., Grigera, S.A., Klemke, B., Castelnovo, C., Moessner, R., Czternasty, C., Meissner, M., Rule, K.C., Hoffmann, J.U., et al. (2009). Dirac strings and magnetic monopoles in the spin ice

Dy2Ti2O7. Science *326*, 411–414. https://doi.org/10.1126/science.1178868.

138. Deguchi, K., Matsukawa, S., Sato, N.K., Hattori, T., Ishida, K., Takakura, H., and Ishimasa, T. (2012). Quantum critical state in a magnetic quasicrystal. Nat. Mater. *11*, 1013–1016. https://doi.org/10.1038/nmat3432.

139. Vedmedenko, E.Y., Grimm, U., and Wiesendanger, R. (2004). Noncollinear magnetic order in quasicrystals. Phys. Rev. Lett. *93*, 076407. https://doi.org/10.1103/PhysRevLett.93.076407.

140. Lu, P.J., and Steinhardt, P.J. (2007). Decagonal and quasi-crystalline tilings in medieval Islamic architecture. Science *315*, 1106–1110. https://doi.org/10.1126/science.1135491.

141. Coombs, D.. https://www.coombscriddle.com/, [Accessed 10 October 2022].

142. Ajlouni, R. (2018). Quasi-periodic geometry for architectural acoustics. ENQUIRY: ARCC J. *15*, 42–61.

143. Bindi, L., Pham, J., and Steinhardt, P.J. (2018). Previously unknown quasicrystal periodic approximant found in space. Sci. Rep. *8*, 16271. https://doi.org/10.1038/s41598-018-34375-x.

144. Sanchez-Palencia, L., and Santos, L. (2005). Bose-Einstein condensates in optical quasicrystal lattices. Phys. Rev. A . (Coll. Park). *72*, 053607. https://doi.org/10.1103/PhysRevA.72.053607.

145. Viebahn, K., Sbroscia, M., Carter, E., Yu, J.C., and Schneider, U. (2019). Matter-wave diffraction from a quasicrystalline optical lattice. Phys. Rev. Lett. *122*, 110404. https://doi.org/10.1103/PhysRevLett.122.110404.

146. Guidoni, L., Triché, C., Verkerk, P., and Grynberg, G. (1997). Quasiperiodic optical lattices. Phys. Rev. Lett. *79*, 3363–3366. https://doi.org/10.1103/PhysRevLett.79.3363.

147. Autti, S., Eltsov, V.B., and Volovik, G.E. (2018). Observation of a time quasicrystal and its transition to a superfluid time crystal. Phys. Rev. Lett. *120*, 215301. https://doi.org/10.1103/PhysRevLett.120.215301.

148. Wilczek, F. (2012). Quantum time crystals. Phys. Rev. Lett. *109*, 160401. https://doi.org/10.1103/PhysRevLett.109.160401.

149. Choi, S., Choi, J., Landig, R., Kucsko, G., Zhou, H., Isoya, J., Jelezko, F., Onoda, S., Sumiya, H., Khemani, V., et al. (2017). Observation of discrete time-crystalline order in a disordered dipolar many-body system. Nature *543*, 221–225. https://doi.org/10.1038/nature21426.

150. Zhang, J., Hess, P.W., Kyprianidis, A., Becker, P., Lee, A., Smith, J., Pagano, G., Potirniche, I.D., Potter, A.C., Vishwanath, A., et al. (2017). Observation of a discrete time crystal. Nature *543*, 217–220. https://doi.org/10.1038/nature21413.

151. Mi, X., Ippoliti, M., Quintana, C., Greene, A., Chen, Z., Gross, J., Arute, F., Arya, K., Atalaya, J., Babbush, R., et al. (2022). Time-crystalline eigenstate order on a quantum processor. Nature *601*, 531–536. https://doi.org/10.1038/s41586-021-04257-w.

152. Flicker, F. (2018). Time quasilattices in dissipative dynamical systems. SciPost Phys. *5*, 001. https://doi.org/10.21468/SciPostPhys.5.1.001.

153. Peng, Y., and Refael, G. (2018). Time-quasiperiodic topological superconductors with Majorana multiplexing. Phys. Rev. B *98*, 220509. https://doi.org/10.1103/PhysRevB.98.220509.

154. Giergiel, K., Kuroś, A., and Sacha, K. (2019). Discrete time quasicrystals. Phys. Rev. B *99*, 220303. https://doi.org/10.1103/PhysRevB.99.220303.

155. Amaral, M.M., Aschheim, R., Bubuianu, L., Irwin, K., Vacaru, S.I., and Woolridge, D. (2017). Anamorphic quasiperiodic universes in modified and Einstein gravity with loop quantum gravity corrections. Classical Quant. Grav. *34*, 185002. https://doi.org/10.1088/1361-6382/aa828a.

156. Bubuianu, L., and Vacaru, S.I. (2018). Deforming black hole and cosmological solutions by quasiperiodic and/or pattern forming structures in modified and Einstein gravity. Eur. Phys. J. C *78*, 393. https://doi.org/10.1140/epjc/s10052-018-5853-6.

157. Hirata, A., Kang, L.J., Fujita, T., Klumov, B., Matsue, K., Kotani, M., Yavari, A.R., and Chen, M.W. (2013). Geometric frustration of icosahedron in metallic glasses. Science *341*, 376–379. https://doi.org/10.1126/science.1232450.

158. Miao, J., Ishikawa, T., Robinson, I.K., and Murnane, M.M. (2015). Beyond crystallography: diffractive imaging using coherent x-ray light sources. Science *348*, 530–535.

159. Huang, X., Zhu, J., Ge, B., Gerdes, F., Klinke, C., and Wang, Z. (2021). In Situ constructing the kinetic roadmap of octahedral nanocrystal assembly toward controlled superlattice fabrication. J. Am. Chem. Soc. *143*, 4234–4243. https://doi.org/10.1021/jacs.0c12087.

160. Huang, X., Zhu, J., Ge, B., Deng, K., Wu, X., Xiao, T., Jiang, T., Quan, Z., Cao, Y.C., and Wang, Z. (2019). Understanding Fe3O4 nanocube assembly with reconstruction of a consistent superlattice phase diagram. J. Am. Chem. Soc. *141*, 3198–3206. https://doi.org/10.1021/jacs.8b13082.

161. Weidman, M.C., Smilgies, D.M., and Tisdale, W.A. (2016). Kinetics of the self-assembly of nanocrystal superlattices measured by real-time in situ X-ray scattering. Nat. Mater. *15*, 775–781. https://doi.org/10.1038/Nmat4600.